



MAGIC-TDAS 10-11  
101125 / D. Garrido

## The effect of aerosol atmospheric profiles on the performance of the MAGIC telescopes.

M. Doro (UAB)

<michele.doro@uab.cat>

D. Garrido (UAB)

<daniel.garrido@uab.cat>

A. Moralejo (IFAE)

<morajelo@ifae.es>

October 25, 2011

### Abstract

In this document we present the results of a study performed during the master thesis of Daniel Garrido concerning the effect of the presence of aerosol overdensities during simulated MAGIC-stereo system observations. We explain how we produced a special set of MC gammas and analyzed them using a modified version of the Reflector program which included several models for the aerosol distribution. Both processes are described. Besides, we study the effect of three aerosol parameters (the overall aerosol density, the density of an aerosol layer and the height of an aerosol layer) on the observed characteristics of the simulated source. The effects on the effective area, migration matrix and estimated spectrum are described, as well as the systematic decrease in the estimated flux and in the estimated spectral index of the simulated source are found, directly correlated with the density of the aerosol layer. Especially adapted MC is used to correct for the presence of aerosols and we recover the originally simulated spectrum, as expected, but an increase in the energy threshold of our telescope system, correlating with the overall trigger rate, is found.

# Contents

<b>1</b>	<b>Introduction</b>	<b>3</b>
<b>2</b>	<b>Description of the simulation</b>	<b>3</b>
<b>3</b>	<b>Aerosol Models</b>	<b>5</b>
<b>4</b>	<b>Results</b>	<b>8</b>
4.1	Elterman models . . . . .	9
4.2	Aerosol layers: the influence of height . . . . .	12
4.3	Aerosol layers: the influence of density . . . . .	14
<b>5</b>	<b>Conclusions</b>	<b>15</b>
<b>6</b>	<b>Outlook</b>	<b>17</b>
	<b>Appendices</b>	<b>24</b>
<b>A</b>	<b>Figures</b>	<b>36</b>
<b>B</b>	<b>Input Cards</b>	<b>36</b>
B.1	Corsika Input Card . . . . .	36
B.2	Reflector Input Card . . . . .	36
B.3	Camera Input Card . . . . .	38

## 1 Introduction

The atmosphere of the Earth can be considered as part of any IACT system because it allows us to determine the energy of the incident particle. Since one of the biggest sources of systematic errors in the energy estimation is the incomplete knowledge of the atmosphere, understanding Cherenkov light propagation through the atmosphere is a key element to reduce the systematic uncertainties of the measurements. The aerosol model, that is currently being used in the Monte Carlo simulations that MAGIC telescopes use, was not specifically designed to reproduce the characteristics of the atmosphere at the MAGIC location.

The aim of this study is to analyze the kind and size of the errors we make because we don't take into account the different aerosol distributions in our MC. We will check what is the effect produced on the spectrum of a steady simulated source that is observed under high aerosol density conditions after analyzing those data using standard, non-adapted MC. We will try to recover the original parameters of the spectrum of the source using both standard and specially adapted so this will prove that some of the data taken under high-aerosol densities that is usually rejected due to bad quality, i.e. low detection rates, can be recovered if we modify our MC to reproduce non-ideal atmospheric conditions. Similar studies for H.E.S.S. [NPR10] using real, bad-weather data show that we can correct some of those data, thus increasing the duty cycle of the telescopes and improving their performance.

The MAGIC telescopes are nowadays being upgraded to improve their sensitivity: the camera of the first telescope, MAGIC-1, will be changed during 2012 for a higher resolution camera like the one that MAGIC-2 has. MC simulations with the new configuration have not been started yet but some studies have been done. During this thesis work we decided that it would be more useful to simulate the telescopes as they will be after the M1-camera upgrade, so the obtained results would be relevant for a longer time. Thus, we modified the necessary parameters in the simulation and analysis chain to simulate a stereo system with the same cameras for M1 than for M2, and we took those parameters directly from the ones that are being used for M2.

Besides, the new MAGIC *elastic LIDAR system*, that will allow us to partially monitorize the aerosol content of the atmosphere at the ORM, could use some of the results presented here. Constraints on the required performance of these remote sensing tools can be extracted, as well as for inelastic/Raman LIDARs and for future IACTs like CTA.

## 2 Description of the simulation

The main steps of the simulation are:

1. Producing 4 M-events at Corsika level, in stereo mode. The energy of these events spreads between 30 GeV and 10 TeV and their differential energy spectrum is a power-law with spectral index  $-2.0$ . The ZA was  $20^\circ$  and the AZ was fixed at  $0^\circ$ . The maximum impact radius was chosen to be 300 m and each shower was used 10 times (CSCAT = 10 0. 30000. in Corsika input cards).

2. Running Reflector software on these events using 7 different aerosol models. The models and its implementation in the Reflector code are described in section 3.
3. Running Camera simulation. The input parameters were modified to simulate the response of the MAGIC cameras *after* the M1 camera upgrade: M2 camera parameters were used to simulate the M1 camera response.
4. Developing a set of calibration and pedestal files according to the new upgraded camera configuration since no official, upgraded files were available.
5. Running the MAGIC analysis chain (callisto, star, superstar, melibea) adapting the parameters for the new configuration as well.
6. Dividing the file for each atmospheric situation into 3 groups: 10% of them were used to train the Random Forest (RF) and to compute the Energy Look-Up Tables (LUTs); another 10% was used as MC for the effective area calculation and the remaining 80% was used as 'real data'. We have also used 0.6 M-events real background data of 1FGLJ0338.8 for the RF training.
7. Computing the differential energy flux of the simulated source (an arbitrary time interval was used) with a simple macro. The computation goes as follows: we count the number of surviving events in the melibea files for a certain aerosol model; we divide them in 30 estimated-energy bins in order to have good statistics in each bin as well as a sufficiently precise binning; finally, we divide them by the effective area at each estimated-energy bin. We did not need to use any unfolding technique because we already applied a correction for the committed error in the energy reconstruction inside the effective area calculation code<sup>1</sup>.
8. In order to simulate the presence of aerosols in the atmosphere, since in MAGIC we always use the same kind of MC to analyze our data, we proceeded in the following way: we analyzed the data produced with a dirty atmosphere but we used the RF, LUTs and effective areas computed with the standard MC (usually summed up as 'wrong MC' in this TDAS). In this way we could see the error we were making by not considering the presence of aerosol overdensities because the MC we used to analyze those dirty-atmosphere data simulates a clean atmosphere so it is not sensitive to them.
9. Later on, we wanted to see what would be the remaining effects even if we had specifically adapted MC for each atmospheric situation. Thus, we generated RF, LUTs and effective areas with a fraction of the MC of each model and we analyze the data with their corresponding model. This is the best situation we could have because the MC used to analyze the data is part of the *very same data*. Nevertheless, this is not a realistic situation: production of MC is a very computer-intensive process and we would need to have a specifically

---

<sup>1</sup>Since the effective area is computed using MC you obtain it as a function of *true* energy. But in the computation of the differential energy flux we need to have the effective area as a function of *estimated* energy. A 'folding' technique was applied to account for the limited accuracy of our telescope using the same macro used to compute the effective area, `collarea.C`. We had to add some extra information for the energy reconstruction: an estimation of the slope of the spectrum. Since we perfectly know the slope of our simulated source, something that does not happens with real observations, this method worked perfectly. If we were working with real MAGIC data we would have had to use a more complex unfolding method. Nevertheless, this is a method that is has been successfully used by other IACTs.

produced sets of MC for each night or even less (since the aerosol content of the atmosphere changes rapidly). Nevertheless, it is useful to compare these two cases (the clean-MC analysis and the adapted-MC analysis) in order to see what is the best performance we would ever be able to achieve from this kind of approach.

### 3 Aerosol Models

The aerosol profile we are currently using in MAGIC is called the **Elterman model**, defined by Louis Elterman in 1963 [Elt64]. It is based on a series of measurements taken near the Chesapeake Bay, between Maryland and Virginia, USA, in 1959. It is a model of what the authors call a 'clear atmosphere', with 25° temperature, 55% humidity at sea level. The profile can be described as a small continental aerosol concentration at sea level of 200 photons/cm<sup>3</sup> followed by an approximately exponential decay with a minor increase between 15 and 25 km above sea level. We can see this model in figure 1 and detailed information about it and about its implementation in the MAGIC software can be found in [Mor03].

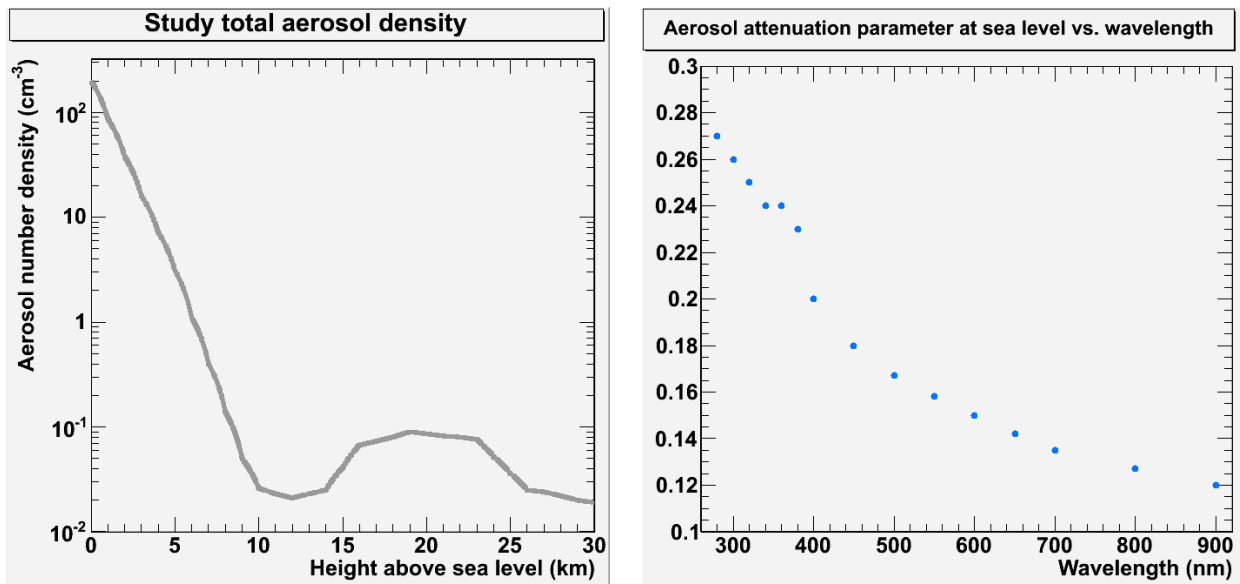


Figure 1: The Elterman aerosol model, the standard profile used inside MAGIC simulations. The first plot is a density profile as a function of height above sea level. The second plot is a direct measurement used in the model of the aerosol attenuation coefficient at sea level as a function of the wavelength.

This profile has been implemented inside the MAGIC software *Reflector*, responsible for the transmission of the Cherenkov photons from their origin inside the air shower to the camera plane. The actual magnitudes taken from the paper from Elterman are the **aerosol number density**<sup>2</sup> as a function of height<sup>3</sup>,  $N(h)$ , and the **attenuation coefficients**<sup>4</sup> at sea level as a function of the wavelength<sup>5</sup>,  $\beta(h, \lambda)$ . We

<sup>2</sup>The variable inside the code is named `aero_n` and its physical dimensions are  $L^{-3}$ .

<sup>3</sup>Its range goes from 0 km to 30 km above sea level in 1 km steps.

<sup>4</sup>The variable is called `aero_betap`, its units are  $\text{km}^{-1}$  and it was measured with a meteorological visibility range of 25 km and an aerosol number density of  $200 \text{ cm}^{-3}$ .

<sup>5</sup>Its values expand from 280 nm to 900 nm using a variable binning.

can see both parameters in figure 1. This second measured parameter describes the extinction profile of light that is traveling through a certain quantity and composition of aerosols suspended in the atmosphere. The  $\beta(h, \lambda)$  values taken from measurements by Elterman are related to aerosols with a continental origin [Elt64].

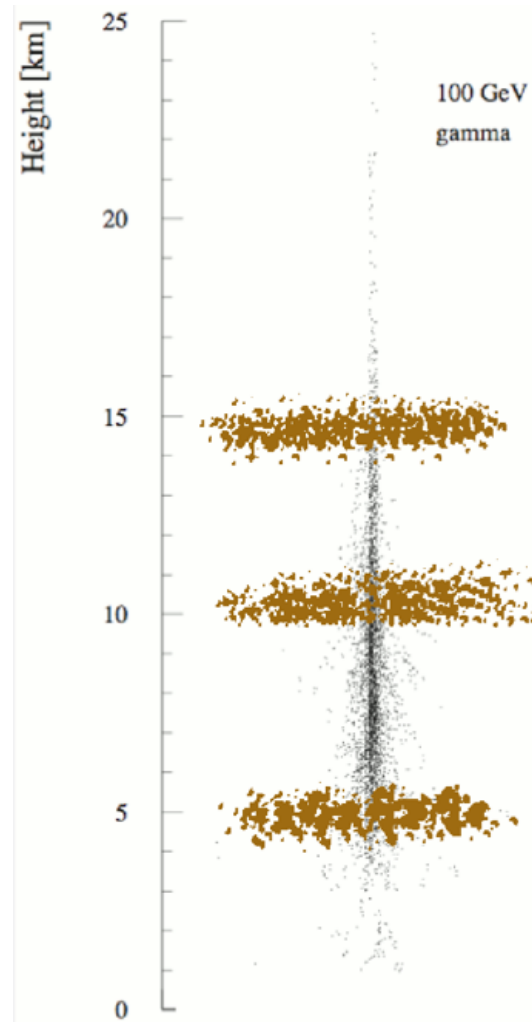


Figure 2: 2-dimensional scheme of an EAS produced by a  $\gamma$ -ray (*black*) and a simplified view of the three aerosol layers that models 4, 5 & 6 simulate (*brown*). The Cherenkov light is emitted between 6 km and 14 km and it peaks around 10 km above sea level [Ber00], so the absorption of these photons by aerosol layers at different heights may vary.

In MAGIC, we have not yet determined what is the effect that aerosols at the MAGIC site produce in the data. In fact, the aerosol content of the atmosphere above the Canary Islands is usually higher than in the Elterman, clean-atmosphere model. Thus, we decided to study the influence of three aerosol-related parameters: overall density, density of a layer and height of a layer. In order to do this we finally decided to simulate 7 aerosol models in addition to the standard one. Each one of them had a name and a numeric code:

- **Changing the overall density:** we multiplied the aerosol density at every height by a factor 15 and 30. We added a multiplicative factor to the variable

`aero_betap` inside the header file `atm.h`<sup>6</sup>. These modified density profiles are plotted in figure 3 (*top left*).

- **Adding an aerosol layer at different heights:** we changed the value of the aerosol density profile<sup>7</sup> to 300 photons/cm<sup>3</sup> in a single bin, at 6,10 and 14 km height each, whereas the aerosol density at other heights was not modified with respect to the standard Elterman profile. Since Cherenkov light is emitted from a wide altitude range, having a layer at different heights should produce different effects. In figure 2 we can easily compare the vertical development of an EAS produced by a  $\gamma$ -ray with the heights of these aerosol layers. This approach has been already used in previous studies [Hru08] but its effect was only seen at the trigger rate level. The corresponding density profiles are plotted in figure 3 (*top right*).
- **Adding an aerosol layer with different densities:** we proceeded in the same way as we did for the previous study, but this time the aerosol layer was added at 6 km height with number densities of 600 and 1200 photons/cm<sup>3</sup> each. These density profiles are plotted in figure 3 (*bottom*).

Model Code	Overall density models	Aerosol Layer models		
		Name	Height (km)	Peak density ( $cm^{-3}$ )
1	Elterman (default)	-	-	-
2	Elterman x 15	-	-	-
3	Elterman x 30	-	-	-
4	-	Low 3	6	300
5	-	Mid 3	10	300
6	-	High 3	14	300
7	-	Low 2	6	600
8	-	Low 4	6	1200

Table 1: Aerosol models used inside Reflector to reproduce a set of simple and realistic atmospheric conditions. Their corresponding density plots are shown in figure 3.

With these models, we wanted to reproduce a simplified version of the usual aerosol distribution at La Palma. To choose the actual values for the parameters we proceeded in the following way. First, we chose the most simple but realistic situations we were able to find in the literature that were physically possible to find at the observatory. The aerosol layers heights and densities were selected taking into account the typical densities of aerosol layers [Ree93, AM05] and their measured heights up to 8 km [SNT<sup>+</sup>10]. All LIDAR measurements we were aware of did not reach higher than this altitude but clouds are known to reach to much higher levels: cirrus, cirrostratus and cirrocumulus can reach even 18 km height [Hru08]. Calima may also reach higher altitudes although no precise studies about this topic have been found. But it is also interesting to see what the effect of this kind of layers will be for the Cherenkov light yield of a shower, on the effective area of our telescopes and on the posterior energy reconstruction of the events. If we find a significant effect it will encourage all groups

<sup>6</sup>MagicSoft/Simulation/Detector/ReflectorII/atm.c, line 104.

<sup>7</sup>Variable `aero_n` inside MagicSoft/Simulation/Detector/ReflectorII/atm.h, line 31

that are developing LIDARs for any IACT experiment to improve present technology in order to be able to detect if there are any aerosol layers as high as 14 km. If no effect is found, then ongoing investigations should not waste too much time and resources trying to improve the altitude range that these LIDAR instruments are able to measure, because, even if an aerosol layer is found, it would not have any measurable effect on the quality of our data.

Secondly, we performed a test for each aerosol model to be sure that the associated transmittance<sup>8</sup> for each atmosphere lied within the MAGIC operating conditions or a little bit beyond them, so the results could also be useful for future IACTs that are expected to work in worse atmospheric conditions. To check the total absorption of the atmosphere, we simulated a set of 500,000 photons between 280 nm and 820 nm (flat distribution) that were coming from outside of the atmosphere (at 100 km above sea level) and above the MAGIC site using the software called `cermaker`<sup>9</sup> and running then `Reflector` on the output. We computed how many of these photons were absorbed, scattered out of the FoV or reflected out of the camera by the mirrors of our telescopes after travelling from the production height to the MAGIC height. Transmittance plots were drawn for each aerosol model (using MAGIC Winter [BHM<sup>+</sup>06] as molecular model), shown in figure 4.

At the same time, we looked for daily extinction measurements in the  $r'$  band ( $\lambda_{eff} \approx 625$  nm) performed by the Carlsberg Meridian Telescope at the ORM. The one with the worst extinction measurements we could find in their online archive<sup>10</sup> was the one measured on July 9<sup>th</sup> 2010, with a value of  $\Delta m = 0.874$ . Therefore, a rough observability limit we can set<sup>11</sup> is that  $T_{lim} = T(\Delta m = 0.874) \approx 0.447$ . This means that any profile with a transmittance below  $\sim 40\%$  at  $\lambda \approx 625$  nm corresponds to an atmospheric situation where MAGIC is operating at extreme observability conditions: the trigger rate for this day is as low as 50 Hz (as retrieved from the daily log files) while the normal trigger rate is about 200 Hz. As we said before and we can see in figure 4 (top right and bottom left), models 3 and 8 are extreme cases because their transmittance at  $\lambda \approx 625$  nm is slightly below this value. The rest of the aerosol models had bigger transmittances, therefore they correspond to more realistic situations.

## 4 Results

In this section, we report the observed effects produced by a high aerosol content of the atmosphere on the MAGIC performance and on the observational parameters of a source. The performance of the telescopes will be characterized by the migration

---

<sup>8</sup>Transmittance,  $T(\lambda, h_1, h_2)$  is the probability of a photon with wavelength  $\lambda$  to travel from a certain height  $h_1$  to a different height,  $h_2$ , for our purpose following a vertical path.

<sup>9</sup>This software can be found in `MagicSoft/Simulation/Detector/ReflectorII/tester/` and one can call it using the command: `cermaker outfilename source_x(cm) source_y(cm) source_z(cm above CT) events`. The coordinates are defined with respect to the center of the 2-telescopes system.

<sup>10</sup>[http://www.ast.cam.ac.uk/ioa/research/cmt/camc\\_extinction.html](http://www.ast.cam.ac.uk/ioa/research/cmt/camc_extinction.html)

<sup>11</sup>Since the extinction is defined as  $\Delta m \equiv m - m_0$  where  $m_0$  is the magnitude of a certain star observed with the best atmospheric conditions and  $m$  is the magnitude of the same star under daily atmospheric conditions. Since  $m = -2.5 \log F + C$ , then  $\Delta m = -2.5 \log(F/F_0)$  and we can compute the transmittance as  $T = F/F_0 = 10^{-\Delta m/2.5}$ .

matrix of our system (estimated energy as a function of true energy of an event), the energy threshold, the efficiency of our simulation (number of events surviving all the simulation and analysis chain divided by the number of produced events) and the effective area. There are two observational parameters that we have studied, both estimated by fitting the differential energy spectrum of our source: the spectral index and the normalization constant.

Besides, we compare the analysis procedures corresponding to two different observational situations: first, we analyze the simulated data with standard-atmosphere MC, that it is used to train the RFs, to create the LUTs and to compute the effective areas; then, we analyze the same data using a subset of these files as adapted MC. The first case corresponds to the actual MAGIC situation, where a single kind of MC, that is not sensitive to the variable aerosol content of the atmosphere, is used to analyze all data. The second case is a check that the analysis method works and it corresponds to the ideal case: the MC simulates the exact atmospheric conditions (we use a part of the very same data), so it is the best MC we could ever produce. This MC represents only a 20% of the total produced data.

As a reminder, we expose the three different aerosol variables whose influence we are studying in the next subsection. First, we compare models 1 (standard, Elterman), 2 and 3 to find out the influence of the overall aerosol density. Then, we compare models 1, 4, 5 and 6 to study the height of an aerosol layer. Finally, models 1, 4, 7 and 8 are compared to study the influence of the density of an aerosol layer.

## 4.1 Elterman models

Comparing the scaled-up versions of the Elterman model (models 1, 2 & 3 in table 1), we can see a notable reduction of the efficiency when the aerosol content is high: only 59% and 31% of the events for model 2 and 3, respectively, manage to trigger the telescope (if compared to the standard model, number 1). Therefore, a light source at high altitudes will look fainter in approximately the same amount as compared with good atmospheric conditions that the Elterman model represents. We will systematically underestimate its real flux if we do not account for the presence of aerosols.

From these efficiencies, we can foresee what is the influence of these aerosols on the effective area of our detector in figure 5 (top) and table 2. We can clearly appreciate a significant decrease of the effective area proportional to the aerosol density, that it affects all energies, but especially the lowest ones. Besides, the energy threshold, understood as the value of the true energy at which  $A_{eff}$  reaches a considerable value, e.g.  $10^4$  m<sup>2</sup>, increases significantly as the atmosphere gets dirtier. For model 3, the telescope is completely unresponsive for all primary  $\gamma$ 's whose energies are below 100 GeV. The physical reason is clear: the lowest energy  $\gamma$ 's produce the dimmest EAS and the presence of a considerable amount of aerosols absorbs most of their Cherenkov light so our detector does not trigger at all. Concerning the high energies the effect of the aerosols is equivalent, but since high energy photons produce the brightest cascades, only the ones that are very far away look dim in the camera; thus, only the far away, high energy EAS stop triggering the telescope system.

The energy reconstruction of the EAS can be seen in the appendix (figure 13). A

Atmospheric Model	Effective area [ $10^3 \text{ m}^2$ ] at different true energies:			
	100 GeV	200 GeV	500 GeV	1 TeV
1: Elterman	$9.13 \pm 0.31$	$26.16 \pm 0.63$	$52.7 \pm 1.7$	$77.9 \pm 2.3$
2: Elterman x 15	$1.27 \pm 0.12$	$16.16 \pm 0.50$	$39.9 \pm 1.5$	$63.6 \pm 2.2$
3: Elterman x 30	$0 \pm 0$	$2.67 \pm 0.21$	$24.7 \pm 1.2$	$45.6 \pm 1.9$
4: Low 3	$3.87 \pm 0.21$	$20.63 \pm 0.56$	$46.0 \pm 1.6$	$70.6 \pm 2.3$
5: Mid 3	$4.26 \pm 0.21$	$20.62 \pm 0.56$	$46.4 \pm 1.6$	$73.0 \pm 2.3$
6: High 3	$6.98 \pm 0.28$	$23.60 \pm 0.60$	$52.3 \pm 1.7$	$78.7 \pm 2.3$
7: Low 2	$0.88 \pm 0.11$	$13.99 \pm 0.54$	$32.3 \pm 1.6$	$58.4 \pm 2.5$
8: Low 4	$0.011 \pm 0.011$	$2.11 \pm 0.19$	$18.5 \pm 1.1$	$34.4 \pm 1.7$

Table 2: Effective area of the MAGIC telescopes at different true energies under the 8 simulated atmospheric conditions. There is an important effective area decrease in the presence of aerosols, especially for the highest density models. The influence of these atmospheric models on the overall energy regim can be seen in figure 5

Model number	Atmospheric Model	Efficiency (%)	Comparison with model 1 (%)
1	Elterman (MW)	4.1	(100)
2	Elterman x 15	2.4	59
3	Elterman x 30	1.3	31
4	Cloud Low 3	3.1	76
5	Cloud Mid 3	3.1	76
6	Cloud High 3	3.6	88
7	Cloud Low 2	2.1	52
8	Cloud Low 4	1.0	24

Table 3: Efficiency of the simulation (number of surviving events divided by number of produced events) for each aerosol model. One can see a major decrease for the models with high aerosol densities but the efficiency remains almost unchanged if we compare models with aerosol layers at different heights.

considerable effect occurs for models 2 and 3: their migration matrices move systematically downwards, below the perfect energy reconstruction line, thus we are underestimating the energy of all the events. There is a 50% and a 70% underestimation<sup>12</sup> of the energy for Elterman x 15 and Elterman x 30 models, respectively. There is also a significant increase of the energy threshold as we can see on the left plots of figure 14: the red points (dirty atmosphere) are systematically shifted rightwards with respect to the black dots (standard atmosphere) and this means that **successful energy reconstruction starts at higher energies**. Comparing the red points in this figure we can see that using adapted-MC, the presence of aerosols increases the energy threshold but we are estimating the energy of the events properly. Looking at any plot in the first row (black points) only for energies above  $\approx 100$  GeV we have an energy bias below 10%. But when we look at the Elterman x 15 model (top left plot, red points) we have

<sup>12</sup>The vertical distance to the line is 0.3 log-units for the Elterman x 15 model and 0.5 log-units for Elterman x 30, i.e.  $E_{true} = 10^x$  and  $E_{est} = 10^{x-y}$  with  $y \approx 0.3$  for the first model and  $y \approx 0.5$  for the second one; in linear units, the relative energy error is then  $\Delta E \equiv (E_{est} - E_{true})/E_{true} = E_{est}/E_{true} - 1 = 10^{-y} - 1$ . Thus,  $\Delta E(y = 0.3) \approx -0.5$  and  $\Delta E(y = 0.5) \approx -0.7$  respectively.

Aerosol Model	$\log_{10} \left[ \frac{dN/dE}{\gamma/\text{GeV}/\text{m}^2} \right]$ at $E = 100 \text{ GeV}$	Spectral Index $-\alpha$
Elterman	$-1.483 \pm 0.011$	$1.985 \pm 0.015$
Elterman x 15	$-1.493 \pm 0.018$	$1.981 \pm 0.015$
Elterman x 30	$-1.502 \pm 0.034$	$1.967 \pm 0.033$
Elterman x 15 (wrong MC)	$-1.677 \pm 0.012$	$2.055 \pm 0.017$
Elterman x 30 (wrong MC)	$-1.926 \pm 0.014$	$2.113 \pm 0.021$

Table 4: Fit parameters of the differential energy spectra of the atmospheric models 1, 2 and 3 to a power-law. The last two fits had an upper energy limit to avoid that the artificial high-energy cut-off modified the estimated spectral slope.

to travel to energies of  $\approx 160 \text{ GeV}$  to find the same energy bias; and for the extreme case, Elterman x 30 (top right, red points), this energy threshold has already reached  $\approx 250 \text{ GeV}$ .

It may seem that a better energy resolution is achieved when we notice that the width of the energy error distributions (right column in figure 13) is smaller for dirty atmospheres than for the standard situation (top right plot in the same figure). However, fluctuations of the estimated energy error are smaller because  $E_{est}$  itself is smaller. And since we are dividing by a fixed  $E_{true}$  value, the overall effect is that the width of this distributions shrinks. A better quantity to know the error on the energy reconstruction is the Mean Squared Error (MSE), that it is defined as the squared sum of the width and the mean, i.e.  $MSE \equiv \sqrt{\sigma^2 + bias^2}$ . This parameter is shown in the third row of figure 14 and there we can see that its value for each model is bigger when we do not take into account the presence of the aerosols (blue points are above the red ones for almost every energy).

The most interesting plot is the differential energy spectrum (figure 6) and also its fit parameters (table 4). Looking at the left side of this figure, we can say that we are perfectly able to recover the original spectra when we are using adapted MC (the best possible MC for this atmospheric situation): **the three models have the same estimated spectral index**. The flux of the fit at 100 GeV is a normalization value we have chosen whose physical interpretation is not trivial and that can change significantly if we choose an energy value different from 100 GeV. We should compare the overall position of the spectrum of a model in figure 6 with respect to the other models. In case we use the standard MC to analyze our data, we obtain the right plot on the same figure. We can see that artificial features are introduced: all points are systematically shifted to the left as a direct consequence of the systematic underestimation of the energy of the primary  $\gamma$ -rays. For the Elterman x 15 model, the flux value at 100 GeV is 35% smaller than the correct MC case<sup>13</sup>; for the Elterman x 30 case, this parameter decreases by 62%. This effect would be translated to a *systematic underestimation of the flux* of a real source if the observations were performed while the aerosol content of the atmosphere was higher than usual. But the interpretation of

<sup>13</sup>The values in the second column on tables 4, 5 and 6 are the differential energy fluxes at 100 GeV and they are written in logarithmic units, i.e.  $\log_{10} \left( \frac{dN_{\gamma}}{dE} \Big|_{100 \text{ GeV}} \right)$ . However, this percentage and the following ones are calculated transforming the values in the table to linear scale. This applies for the rest of the differential energy flux comparisons in this chapter.

this parameter is not trivial because it involves the energy reconstruction of the events, so further investigation of this effect would be needed in order to extract a consistent set of unambiguous physical interpretations. Also the slope or spectral index of our source has notably changed, softening<sup>14</sup> the spectrum: for the Elterman x 15 case, the spectral index decreases by 4% with respect to the adapted MC case; in the most extreme case, Elterman x 30, the steepness of spectrum is increased (in absolute value) by more than 7% of the original spectrum slope, from  $-1.967$  to  $-2.113$ , two results that are not compatible if we take into account their errors bars.

Besides, the migration of events from one energy bin to another in the differential energy plot has two contributions. On the one hand, the energy of the events is systematically underestimated because the high aerosol density makes them look fainter, so events move *from right to left* in the spectrum plot. On the other hand, the effective area is overestimated because we do not take into account the decrease in the true detection area of our system due to the presence of aerosols (figure 5 and table 2). Since the flux is proportional to the *inverse* of the effective area, events move *downwards* in the differential energy spectrum plot. The combination of these two effects produces a **diagonal migration** of the events (downwards, leftwards) at all energies and this can be seen in the lower-energy end of the spectrum: note that on the right plot of figure 6 that there is one extra blue (Elterman x 15) and two extra pink points (Elterman x 30) with smaller energies than the lowest-energy event of the standard spectrum (black points, Elterman); these events are properly reconstructed in the left plot using the right MC, so the energy thresholds of our detector are effectively increased. At the same time, this migration of events produces another effect at the high-energy end of the spectra: an even bigger underestimation of the flux. This is an artifact due to the fact that the energy of the simulated photons was limited to 10 TeV. There are no events with energy above 10 TeV that are able to migrate towards lower energies and an **artificial high energy cut-off** is produced. These two effects will also appear in the spectrum analysis of the next two aerosol studies.

## 4.2 Aerosol layers: the influence of height

We compare now the results obtained for models 4, 5 and 6. The fraction of surviving events (efficiency in table 3) is almost the same for the low (4) and mid (5) altitude models: about 75% w.r.t the default, Elterman model; but this fraction goes up to 86% for the high altitude aerosol layer (model 6). This difference has its cause in the typical Cherenkov production height: the maximum shower development occurs at around 10 km height, so the major part of the Cherenkov photons are produced *below* this aerosol layer located at 14 km above sea level. Only the small fraction that is produced *above* the layer can be affected so this explains why High 3 does not reduce the number of surviving events so drastically. Low 3 and Mid 3 models have so similar event numbers, because most of the Cherenkov photons are produced above these two layers, so the total absorption of photons is the same no matter where the aerosol layer is located.

Aerosol layers at different heights have also varying effects on the effective area but not as severe as in the previous study. Looking at figure 5 (center) and table 2, one

---

<sup>14</sup>A power-law spectrum is *soft* if its spectral index is large (in absolute value) because it means that there are less high energy events. If this index is closer to zero, the spectrum is called *hard* because there is a big number of high energy events.

Aerosol Model	$\log_{10} \left[ \frac{dN/dE}{\gamma/\text{GeV}/\text{m}^2} \right]$ at $E = 100 \text{ GeV}$	Spectral Index $-\alpha$
Elterman	$-1.483 \pm 0.011$	$1.985 \pm 0.021$
Low 3	$-1.476 \pm 0.015$	$1.991 \pm 0.018$
Mid 3	$-1.478 \pm 0.015$	$1.993 \pm 0.018$
High 3	$-1.475 \pm 0.013$	$1.993 \pm 0.016$
Low 3 (wrong MC)	$-1.589 \pm 0.019$	$2.044 \pm 0.016$
Mid 3 (wrong MC)	$-1.646 \pm 0.012$	$1.966 \pm 0.016$
High 3 (wrong MC)	$-1.548 \pm 0.016$	$1.958 \pm 0.015$

Table 5: Fit parameters of the differential energy spectra of the atmospheric models 3, 4, 5 and 6 to a pure power-law. The last three fits had an upper energy limit to avoid the artificial high-energy cut-off to modify the estimated spectral slope (the previous section, 4.1).

can see that the effective area is in fact reduced by the presence of an aerosol layer, especially for a low altitude layer (green histogram). This is what we would physically expect: the lower the aerosol layer, the bigger the number of photons that have to travel through it and having a chance of being absorbed. Thus, the effect of the High 3 model on the effective area is much smaller compared to the Low 3 or Mid 3 models and the lowest energies are especially affected: showers from low energy  $\gamma$ -rays develop higher in the atmosphere, so Cherenkov light has to travel through a bigger fraction of the atmosphere. Besides, there is very little difference between having an aerosol layer at 6 km height or at 10 km height: the blue and the green areas are almost completely overlapping, except for a small difference at energies below 80 GeV.

All three migration matrices are similar too, as we can see in the left column of figure 15, so the dependence of the energy reconstruction on the height of the aerosol layer is small. Only a small energy underestimation for the low altitude layer was found. The relative energy error plots in figure 16 and their fitting parameters in figure 17 show that, while the high altitude layer produces almost no visible effect (figure 16, third row and overlapping points in figure 17, third column), the intermediate and the lower altitude layer show a significant increase of the energy bias. There is a systematic  $\sim 25\%$  underestimation of the energy for the Low 3 when we use uncorrected MC, a  $\sim 15\%$  underestimation for Mid 3 and less than a  $\sim 5\%$  for High 3<sup>15</sup>. This, together with the downwards shift of the migration matrixes, is the evidence that **we are systematically underestimating the energy of the events** if observations are performed under high-aerosol-concentration conditions, especially at low altitudes. Besides, the MSE is almost unchanged for mid and high altitude layers (the third row of figure 17), even if we analyze the data using standard MC (below 25% increase). Only in the low-altitude-layer case, the MSE of the uncorrected data is about 50% bigger than the MSE of the corrected data.

Finally, the overall effect on the reconstructed differential energy spectra for these three cases can be seen in figure 7. If we look at the left plot, we can see that all three cases converge to a single spectrum when we use the properly adapted MC. The spectral

<sup>15</sup>These values are a direct estimation of the distance between the blue and the red dots on the first row plots of figure 17.

index values obtained with the correct MC (see table 5) are statistically compatible with the original  $-2.0$  slope and the flux at 100 GeV is almost equal between the three models (considering their error bars). All of them are compatible with the no-layer, Elterman case. But if we use standard MC, we are producing notable changes in the spectral slope of the simulated source: a 3% increase for the Low 3 model, whereas the spectral indexes for mid and high altitude layer models stay almost unchanged (about 1% increase). But the changes in the normalization parameter are more important: a 9% and a 21% decrease in the flux at 100 GeV for the first two models respectively and while only smaller than 5% decrease for the third model.

### 4.3 Aerosol layers: the influence of density

We can compare models 4, 7 and 8 to look for the influence of the density of the aerosol layer. Looking at table 3, we can see a clear decrease of the number of surviving events as we increase the aerosol density: for the lowest density layer (model 4), only 76% of the events are left, compared with the clean atmosphere (1); 51% and 24% of the events survive when the denser layers (7 and 8 respectively) are located above our telescopes. The migration matrixes (figure 18) also show a severe increase of the energy threshold: events below  $\approx 60$  GeV and  $\approx 125$  GeV for 7 and 8 models respectively are not there any more: the lowest energy events always emit less Cherenkov light so it is easier that, after travelling through the aerosol layer, the observed EAS is so faint that it does not trigger the telescopes. High energy events suffer the same effect but, since they are intrinsically brighter, only showers very far away from the telescopes will look faint in the camera and may not be detected.

In figure 20, we find that the energy threshold for model Low 3 has risen up to 125 GeV, for model Low 2 is now 160 GeV and it is as high as 250 GeV for the highest density model, Low 4. If we now compare the first plot on the right column of the same figure 18, with the two plots below, we see the combination of two effects: as before, the lowest energy events are not detected by the telescopes but, since we are now using the standard MC, we underestimate their energy so we end up counting for events whose wrongly reconstructed energy is below the true energy threshold of our detector. We can see this effect easily because the distance between the perfect-energy-estimation line ( $E_{est} = E_{true}$ ) and the migration matrix implies a  $\sim 25\%$  energy underestimation for model 4, a  $\sim 50\%$  underestimation for model 7 and a major  $\sim 70\%$  underestimation of the energy of the events for model 8. All these physical interpretations can be also extracted from the plot of the energy estimation error (figure 19) and their fit parameters (figure 20).

We should finally see the reconstructed differential energy spectrum obtained with these three models (figure 8, using the adapted MC on the left and using the standard MC on the right). We again recover the original spectra when we correct for the presence of these aerosol layers in our MC, but drastic modifications are introduced if we do not take them into account: a 23% decrease in the for Low 3, a 29% reduction for Low 2 and a 65% decrease for Low 4. Nevertheless, maybe the most interesting effect is the variation of the spectral index of this source when we do not adapt our MC: it decreases a  $\approx 3\%$  for Low 3, a  $\approx 7\%$  for Low 2 and a major decrease of  $\sim 16\%$  for Low 4. Therefore, spectral indexes could be underestimated up to a  $\approx 16\%$  if a low-altitude aerosol layer is located above the observatory during data taking.

Aerosol Model	$\log_{10} \left[ \frac{Flux}{\gamma/\text{GeV}/\text{m}^2} \right]$ at $E = 100 \text{ GeV}$	Spectral Index $-\alpha$
Elterman	$-1.483 \pm 0.011$	$1.985 \pm 0.015$
Low 3	$-1.476 \pm 0.015$	$1.991 \pm 0.018$
Low 2	$-1.494 \pm 0.022$	$1.998 \pm 0.024$
Low 4	$-1.514 \pm 0.040$	$1.991 \pm 0.039$
Low 3 (wrong MC)	$-1.589 \pm 0.019$	$2.044 \pm 0.016$
Low 2 (wrong MC)	$-1.642 \pm 0.012$	$2.132 \pm 0.017$
Low 4 (wrong MC)	$-1.966 \pm 0.014$	$2.301 \pm 0.023$

Table 6: Main parameters of the power law fit of the differential energy spectra for the atmospheric models 4, 7 and 8. Again, the last three fits had an upper energy limit to avoid the artificial cut-off to modify the estimated spectral slope (explained at the end of section 4.1).

A general comment about all the spectra obtained with the different models is needed: usually, MAGIC publications describing the observation of a source are giving the spectral index with a systematic uncertainty of 0.20 at least. The biggest deviation from the simulated spectra that we have found is a  $\approx 7\%$  of a  $-2.0$  spectral index, thus a systematic underestimation of  $\approx 0.14$  under extreme atmospheric conditions<sup>16</sup>. This shows that the poor knowledge of the atmospheric influence on IACTs performance is a known weakness that IACTs already account for in the error estimation of the parameters of a source. If we were able to precisely characterize and to correct for these systematic effects, a better physical description could be done of the observed sources and stronger constraints could be set on theoretical models.

## 5 Conclusions

As a sum up of the main conclusions that we have been able to produce with our MC simulation study, we should mention the following achievements:

- We have prepared a set of software tools that were needed to study the influence of different atmospheric conditions on the performance of the MAGIC telescopes using MC simulations. With the acquired knowledge we can now simulate as many atmospheric situations as needed regarding the aerosol distributions. Any further investigation on this topic will be now much easier. We would like to emphasize that some of the results presented are preliminary and they need further investigation. However, we have already been able to find some clear effects caused by the presence of aerosols when we do account for them in the MC used to analyze those data.
- The biggest influence on the performance of the MAGIC telescopes comes from the number density of the aerosols. As expected, we have found that **the higher the aerosol density is, the smaller becomes the detector effective area and the bigger the energy threshold**, and we have quantified this effect in a

<sup>16</sup>Low 4 model shows a stronger variation of the spectral index, but this model corresponds to an extreme situation which MAGIC is not actually able to observe.

few cases: an increase of the overall aerosol density of a factor 15 leads to a 60% increase of the energy threshold; for a factor 30, the energy threshold rises up by 150%. Two effects were found for the reconstructed differential energy spectrum that could be corrected for, if we adapt our MC. First, a **systematic underestimation of the source intrinsic flux** by 45% and 65% for each model, respectively, if compared with the fluxes we would obtain using our perfectly adapted MC. The second effect is a softening, i.e. **steepening of the differential energy spectra**: a decrease in the estimated spectral index of our observed source between 3% and 6%.

- Aerosols are usually structured in several layers at different heights, with different densities and different compositions. In order to simplify all these possible situations, we simulated six aerosol models based on the Elterman aerosol model and adding an extra aerosol layer to it. They were divided in two groups: three models with the same aerosol over-density but located at different heights and another set of three models with layers located at the same altitude but with different densities. This has allowed us to estimate how several observational parameters change when the density or the height of the aerosol layer varies. In order to derive a solid dependency of the observational quantities on these two parameters, a finer binning of the aerosol parameters would be needed. This can be done easily now that we have developed the necessary software tools, provided the necessary CPU-time.
- The performance of the MAGIC telescopes **showed a major difference when a high, a mid or a low altitude aerosol layer is present**. A high altitude layer at 14 km height has little influence in the development of the EM shower induced by a  $\gamma$ -ray, but lower aerosol layers have been found to produce significant effects: the effective areas at low energies are significantly reduced and this fact results into an up to 20% underestimation of the flux of the source for the case of a layer at 6 km above sea level. There is also a bigger systematic underestimation of the energy of the primary  $\gamma$ -rays the lower the aerosol layer is. Besides, no significant variation of the estimated spectral index for any of these three aerosol layers was found. This translates directly into the need for a LIDAR system able to detect and characterize aerosol layers up to 10 km height, but higher measurements are not needed to correct the observational data.
- Nevertheless, the transmittance profiles produced by these three atmospheric models were exactly overlapping. This shows how important it is for the IACT technique to have more detailed information about the quality of the atmosphere than a single, integrated, extinction factor. Differential information is needed if we want to correct data taken under adverse atmospheric conditions and we have proven that this could be done because we have been able to recover the original spectrum by using special MC. This result confirms the necessity of a fully operating LIDAR system and a long-term study of the atmospheric conditions that this instrument is able to provide.
- When we fixed the height of the aerosol layer and we only modified its number density, we observed major changes in all the studied observational parameters. For a layer with 600 photons/cm<sup>3</sup> we have found that we do not detect  $\sim 50\%$  of the events that were detected by the telescopes in the no-layer case. In the

extreme case of 1200 photons/cm<sup>3</sup> density layer, we only detected 20% of the photons that were detected in the standard, clean-atmosphere situation. The threshold for a proper energy estimation is notably risen to 160 and 250 GeV for each model respectively and the effective area is severely reduced. Besides, there was **a significant underestimation of the energy of the events up to 70%, an underestimation of the flux of the source up to 65% and an up to 15% steepening of the observed spectrum for extreme atmospheric conditions.** Therefore, all these results confirm that the major influence on the performance of IACTs is the aerosol density and that **it is possible to correct for these effects using properly adapted MC.** We want to especially emphasize this significant variation of the spectral index of the source when high aerosol densities are present at the location of the telescopes. After a deeper analysis, these results could be used as positive crosscheck of previous studies like [Nf09].

- Our work has confirmed the **systematic underestimation of the flux of a source** when a high aerosol concentration is found and we also have been able to quantify the error on the estimated performance parameters if we are oblivious of the presence of these aerosols when we analyze the experimental data. A recent study [Nf09] claimed that they had observed a modification of the source spectral index using simulation methods similar to ours. We have confirmed the **steepening of the spectrum of a source observed during high aerosol densities situations.** Nevertheless, the differences between the aerosol models used here and in [Nf09] have to be looked at more carefully to see if both results are compatible within each other.

## 6 Outlook

Finally, we will try analyze which part of this study needs deeper analysis and what are the next steps we think any future investigation on this topic should follow.

We have included an extra modification with respect to the standard MC simulations within MAGIC that we have not analyzed in this TDAS: we have modified the MAGIC-1 Camera input parameters to simulate the new Camera hardware that is planned to be installed at La Palma on November 2011 and that will allow MAGIC to end up with two twin telescopes.

Another analysis that could not be included here was the effect of these atmospheric models on the image parameters to better understand and confirm how the atmosphere composition affects the shower development. It would be interesting to investigate this topic because it would probably be the first of its kind: a detailed study of the aerosol influence on IACT image parameters has never been published and their conclusions will likely be easy to extrapolate to other projects in this field.

We are also aware of the limited resemblance of the simulated aerosol models with the real situations at the observatory site: aerosol distributions are usually multilayered, with very varied density profiles and compositions. Our models are a deliberated simplification of all these characteristics into a set of models whose goal was the study of the influence of just a single parameter at a time and it allowed us to extract specific

conclusions that would be harder to find if we had used complex but realistic aerosol distributions. We wanted to simplify as much as we could these situations but using realistic values of the parameters of each model. We performed several checks on a bigger set of models to select the most plausible candidates, that were the ones presented here. A future step would be to develop highly realistic models that resemble the measured atmospheric conditions at La Palma. This could be done using LIDAR data that the MAGIC Collaboration is starting to collect on site and developing some specific software to analyze this data and implement it into the MAGIC simulation software.

A final and highly-desired step would be to implement corrections on observational data that are usually discarded because of the bad quality of the data. A future goal would be to be able to correct these data through the usage of aerosol-corrected LUTs and RFs or via predefined, average models like MAGIC Winter and MAGIC Summer molecular models are now implemented in the standard simulation chain. In this way, the effective and limited duty cycle of ground-based Cherenkov telescopes could be significantly increased.

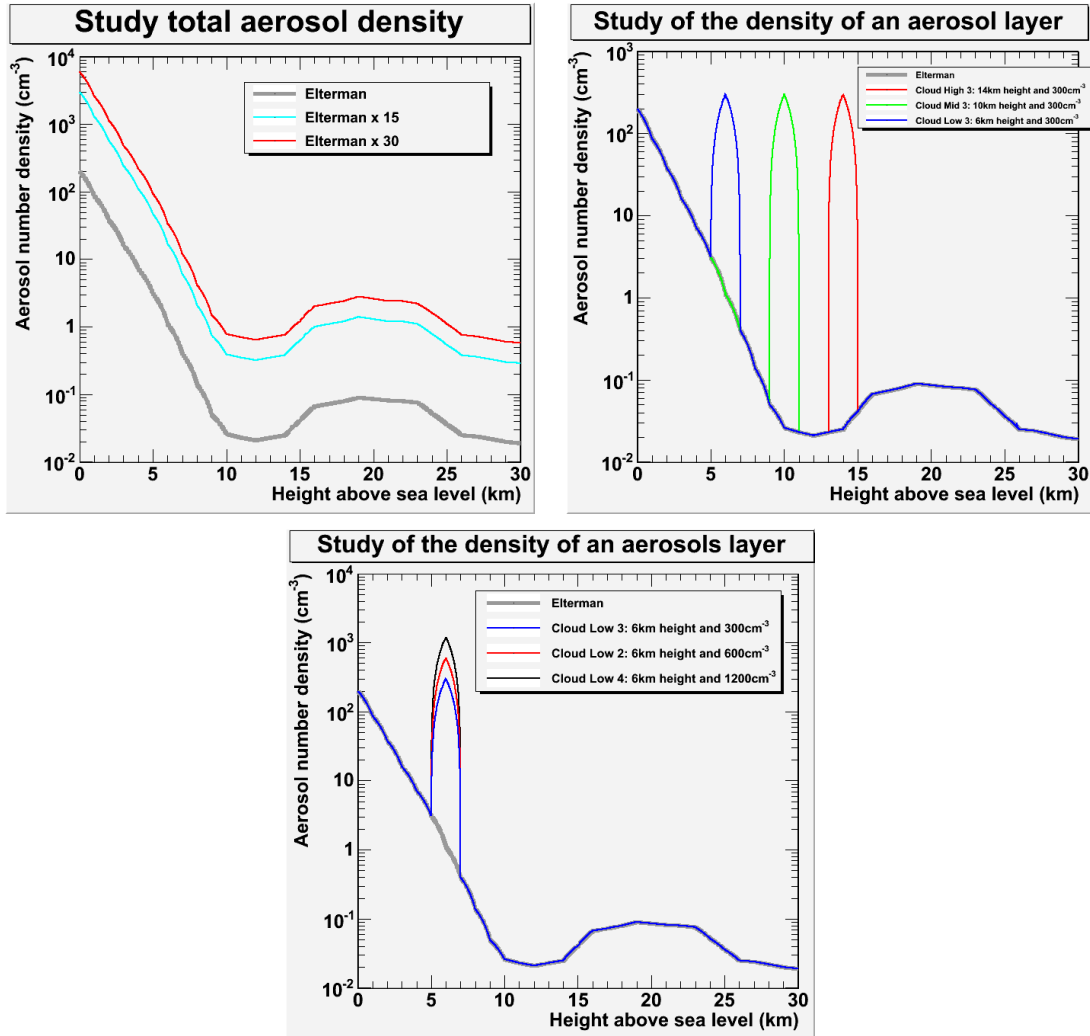


Figure 3: *Top left:* Aerosol density as a function of height for the standard model and the two scaled versions of the Elterman model. *Top right:* Aerosol density as a function of height for three models with aerosol layers at different heights but with the same density. *Bottom:* Aerosol density as a function of height for three models with aerosol layers of different densities. The standard Elterman profile is also plotted for comparison (thick grey) in all these plots. The density values for models 4-8 (*top-right* and *low*) was only modified in a single bin. However, Reflector interpolates linearly to produce a finer binning, so the modification spreads over two bins. Besides, the overdensity does not look triangular but curved, because we are using a logarithmic scale.

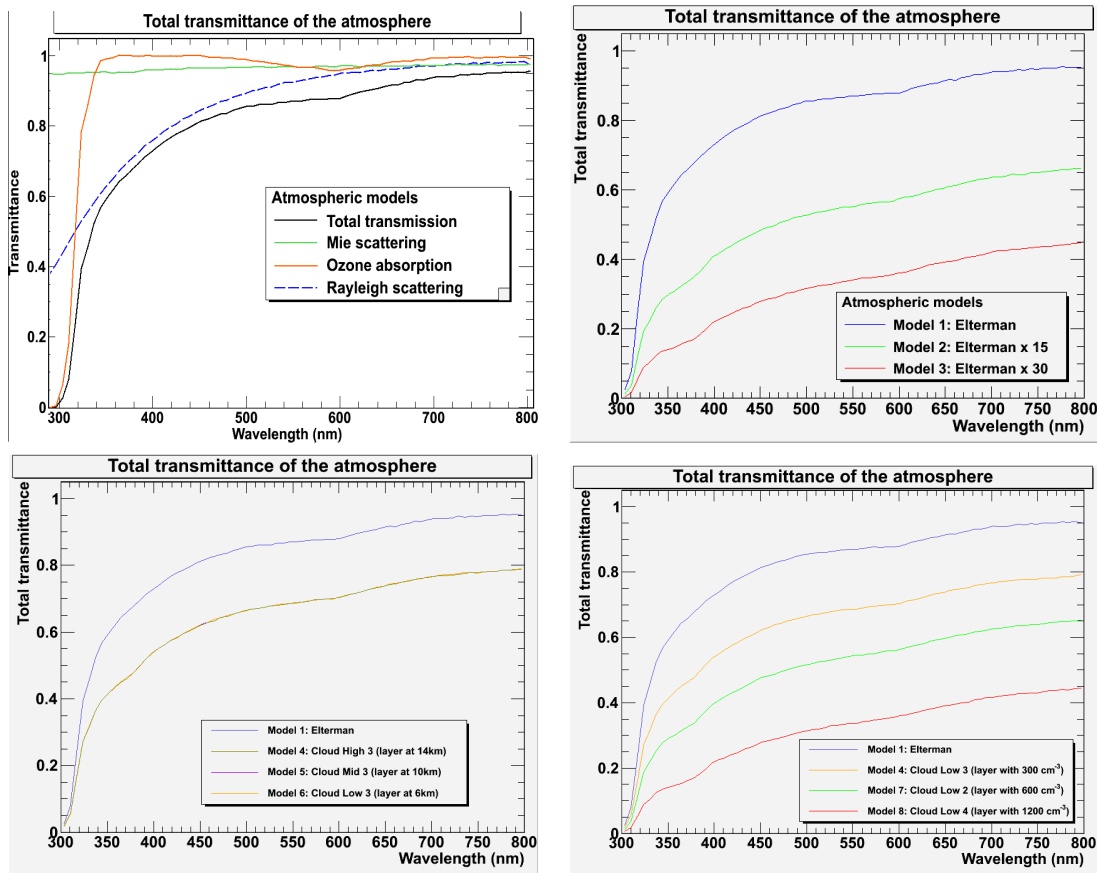


Figure 4: *Top left:* Transmittance of light from 100 km to 2.2 km with the standard MAGIC atmosphere (blue, Rayleigh scattering by the molecular component; green, Mie scattering by the Elterman aerosol model; orange,  $O_3$  absorption; black, total absorption as the sum of the previous three components). *Top right:* Transmittance of light from 100 km to 2.2 km through the atmosphere with the Elterman, Elterman x 15 (green) and Elterman x 30 (red) aerosol models. *Bottom left:* Transmittance of light between 100 km and 2.2 km for no atmosphere case (black), standard (blue), High 3 (red), Mid 3 (purple) and Low 3 (orange). Note that all these three models produce the same transmittance curve because the only difference among them is the height of the extra aerosol layer and, since the density of this layer is the same in all three models, the same effect on the total transmittance is produced. Since we only compute the integral probability of an optical photon to travel from outer space until the height of the telescope, it does not matter where we put our aerosol layer. This does not mean that all these cases will be the same from the point of view of Cherenkov light transmission because every Cherenkov photon in an EM shower is produced at a different height, so layers at different heights will produce a different effect on the same EM cascade. *Bottom right:* Transmittance of light between 100 km and 2.2 km for the Elterman case (blue, just for comparison) and also for Low 3 (orange), Low 2 (green) and Low 4 (red) models.

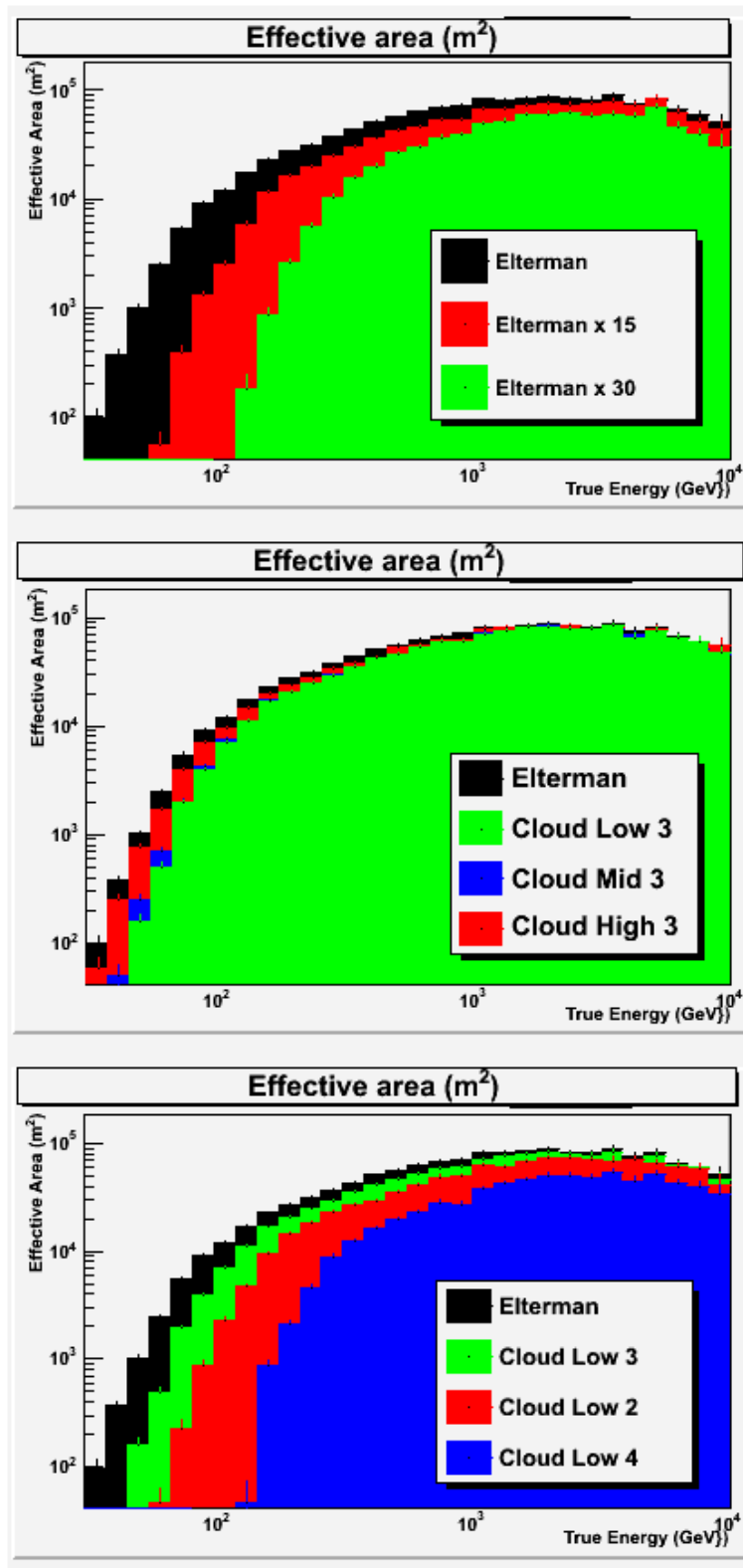


Figure 5: Effective area as a function of the true energy of the primary particle for models 1, 2, 3 (top), models 1, 4, 5, 6 (center) and models 1, 4, 7, 8 (down).

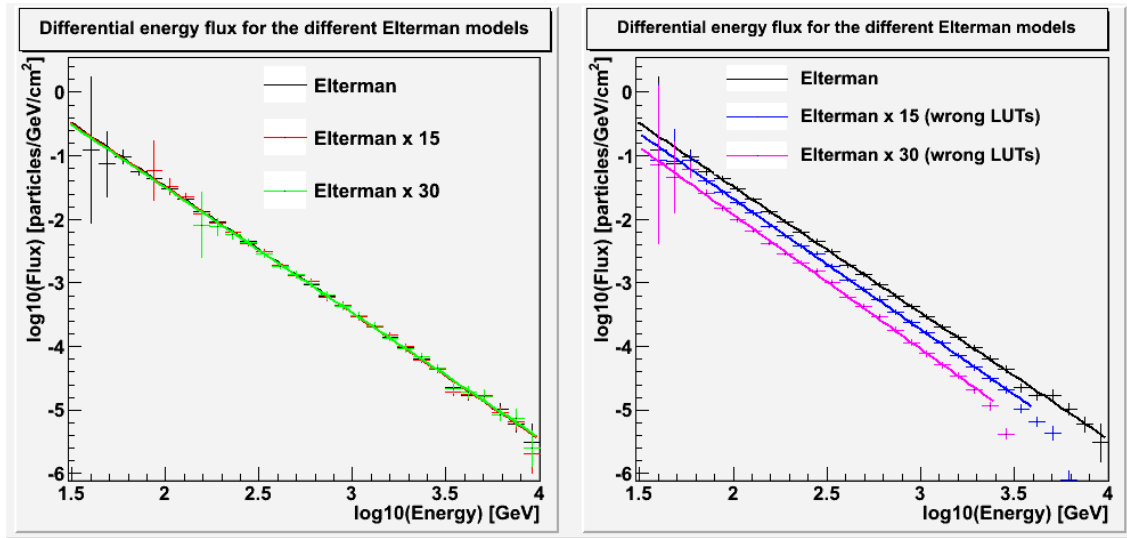


Figure 6: *Left*: Differential energy spectrum for the three different versions of the Elterman model (1, 2 and 3) using adapted MC for the analysis. *Right*: The same data analyzed using standard MC, without taking into account the presence of aerosols. The high energy cut-off is an artificial effect that is explained at the end of this section.

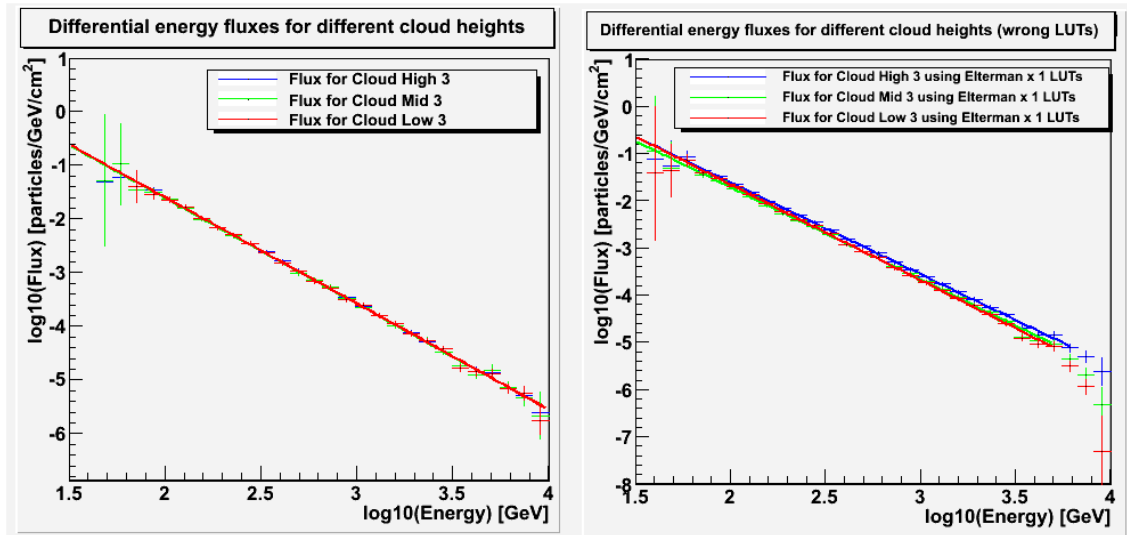


Figure 7: *Left*: Differential energy flux for the three different aerosol layer models with different heights (4, 5 and 6) using adapted MC for the analysis. *Right*: The same data analyzed using standard MC, without taking into account the presence of additional aerosols. The high energy cut-off is an artificial effect that we explained at the end of section 4.1.

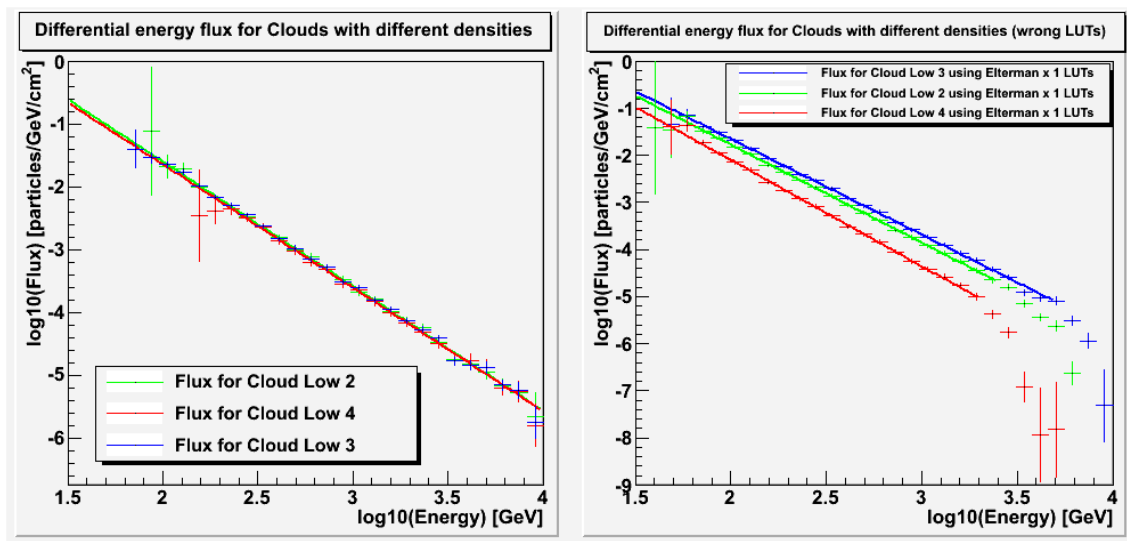


Figure 8: *Left:* Differential energy flux for the three aerosol layer models with different densities (4, 7 and 8) using adapted MC for the analysis. *Right:* The same data analyzed using standard MC, without taking into account the presence of aerosols. The high energy cut-off is an artificial effect that it is explained at the end of section 4.1.

# Appendices

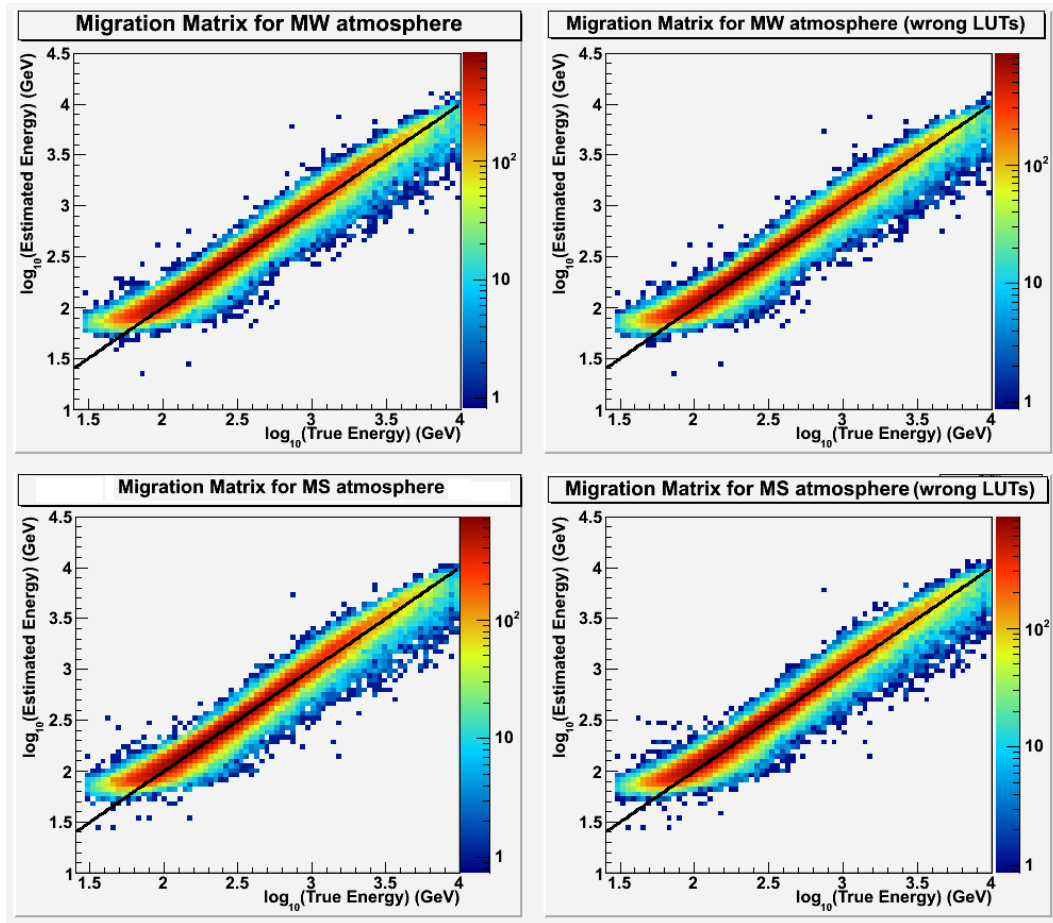


Figure 9: Estimated energy vs True energy (migration matrix) for MW (left) and MS (right) models. A diagonal line ( $E_{est} = E_{true}$ ) is drawn to compare.

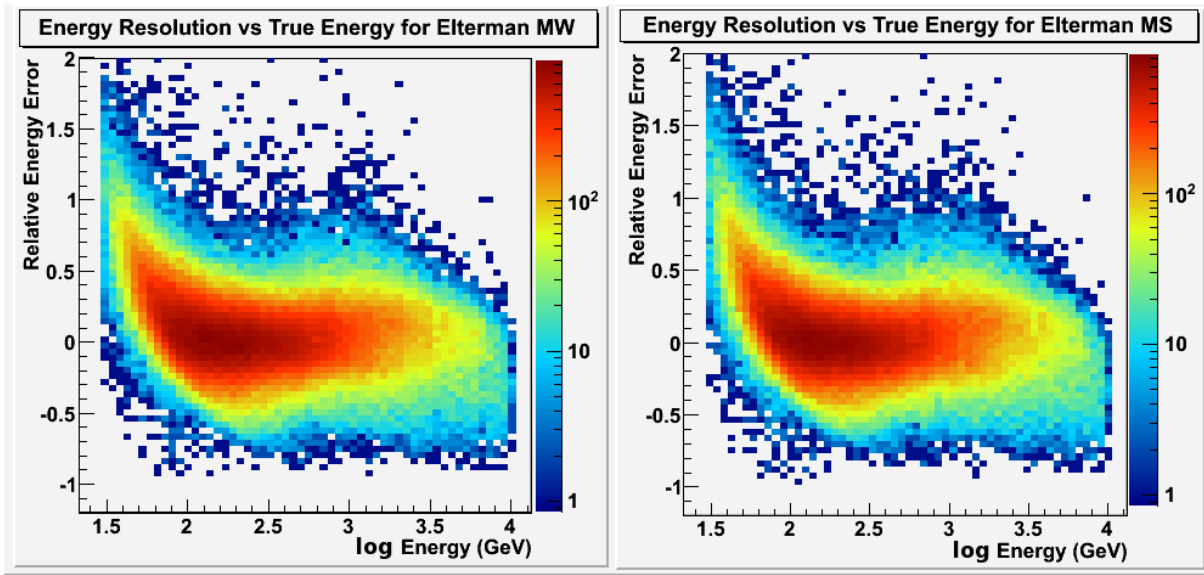


Figure 10: Relative energy error,  $\frac{E_{est}-E_{true}}{E_{true}}$ , as a function of the true energy for MW model (left) and MS model (right).

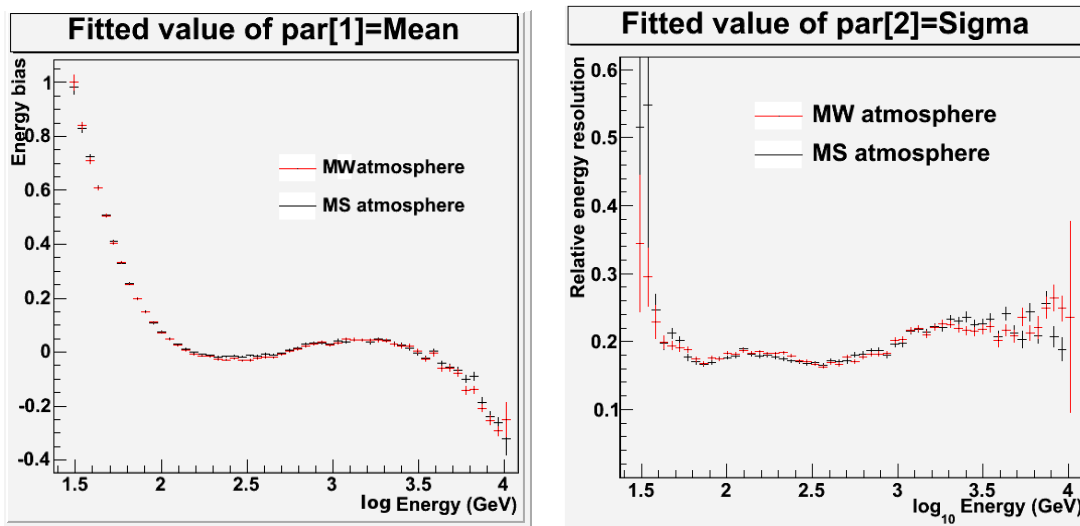


Figure 11: Mean (Square root of the variance,  $\sigma$ ) of the gaussian fit of the relative energy error as a function of energy is represented in the left (right) plot. It is an estimator of the energy bias (resolution) of the detector. MW model (red) and MS model (black) are compared here.

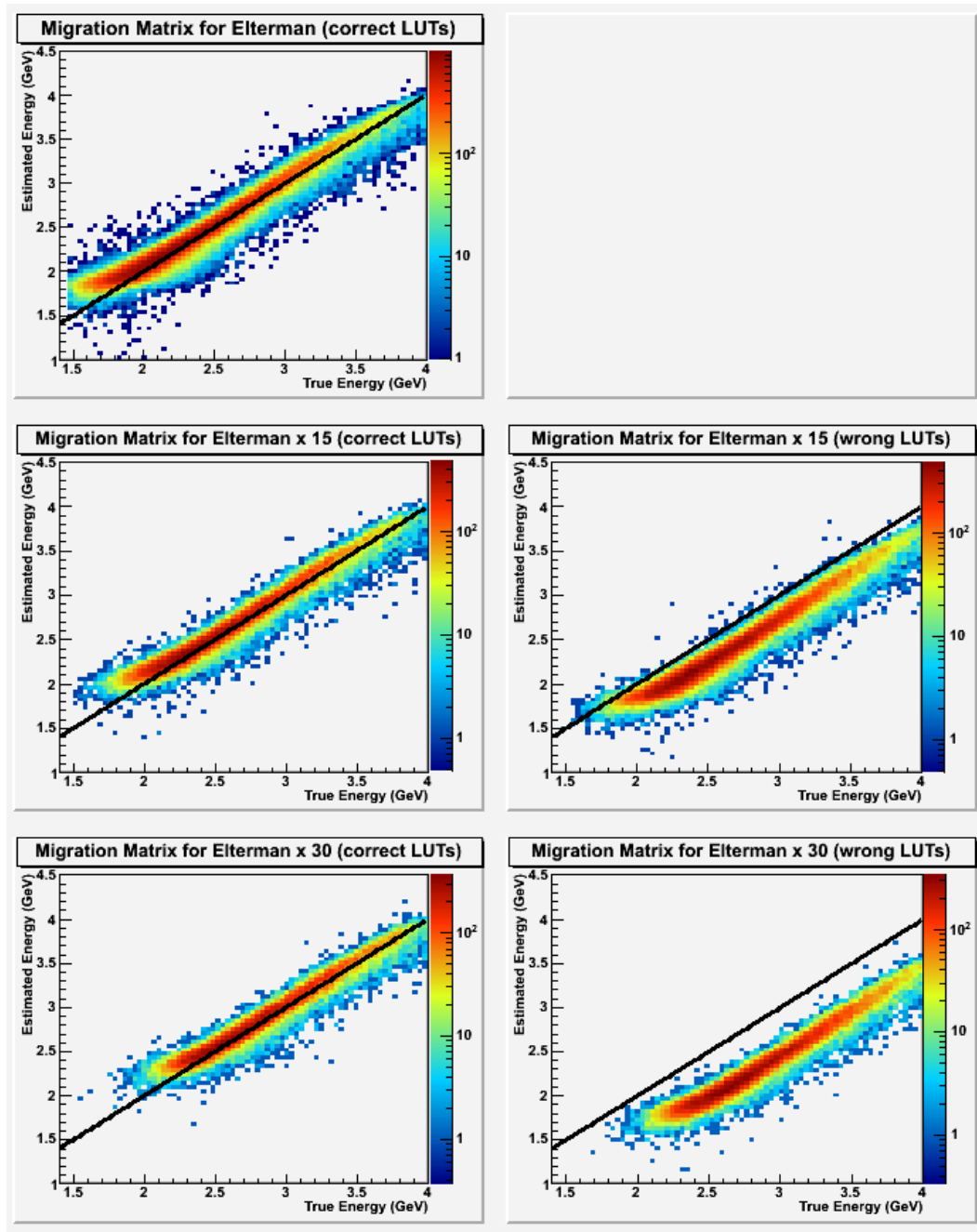


Figure 12: Estimated energy vs True energy (migration matrix) for model 1 (top), 2 (center) and 3 (down). The left column are the events analyzed with the proper MC and the column on the right are the same events but processed with standard MC (model 1). A diagonal line ( $E_{est} = E_{true}$ ) is drawn to compare with the perfect energy reconstruction case.

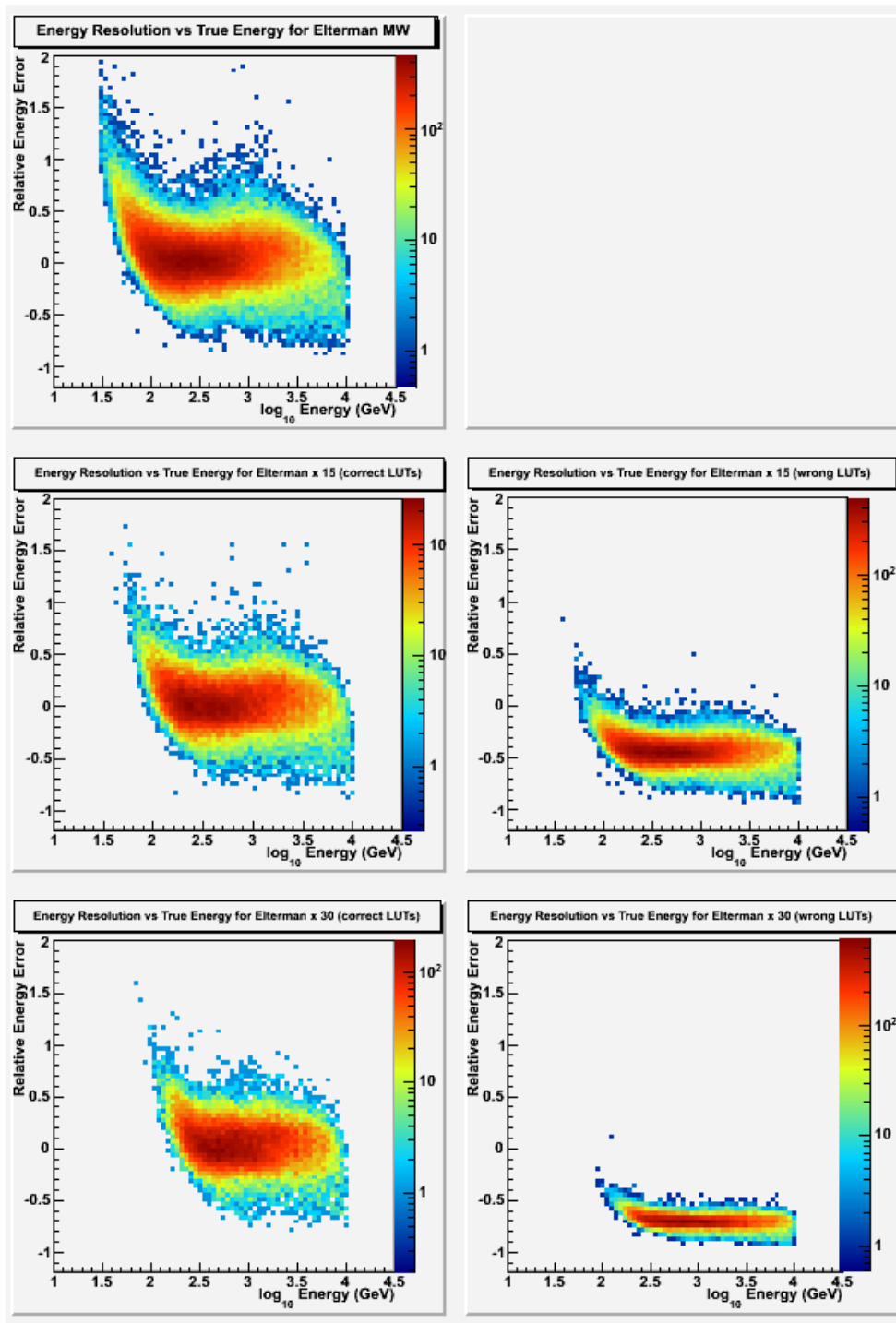
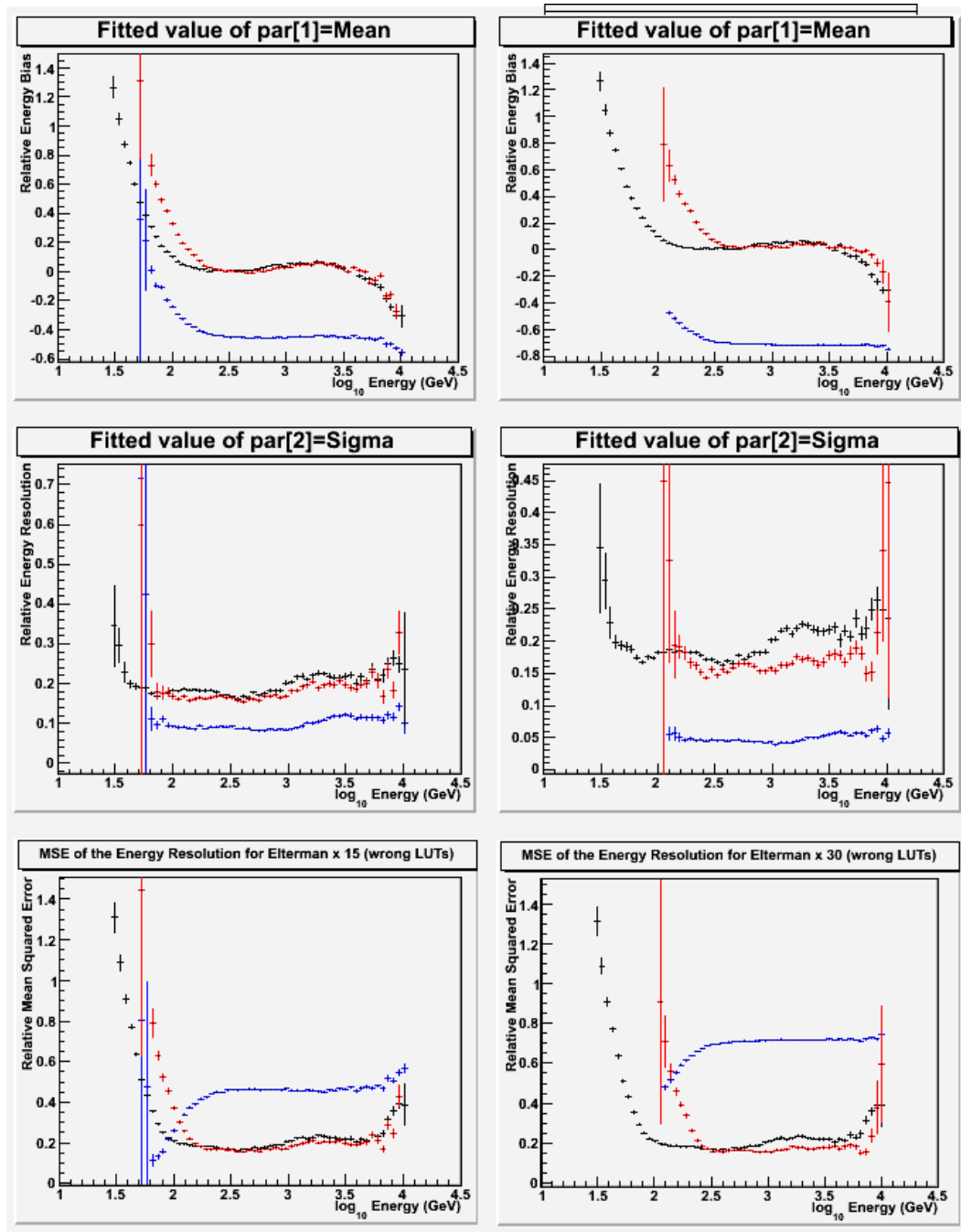


Figure 13: Relative energy error as a function of the true energy in two cases: simulated data analyzed with a properly adapted MC (*left*) and the same data analyzed with standard, model 1 MC (*right*). First row corresponds is the relative energy error for the standard case (model 1), the second row is the Elterman x 15 case (model 2) and the third row is the Elterman x 30 case (model 3).



Model 2: Elterman x 15    Model 3: Elterman x 30

Figure 14: Relative energy bias (first row), relative energy resolution (second row) and relative mean squared error (third row). Black points represent the standard model (Elterman, model 1), red points represent models 2 and 3 for each column respectively but using adapted MC and blue points represent the same models but using standard MC (model 1) to analyze the data.

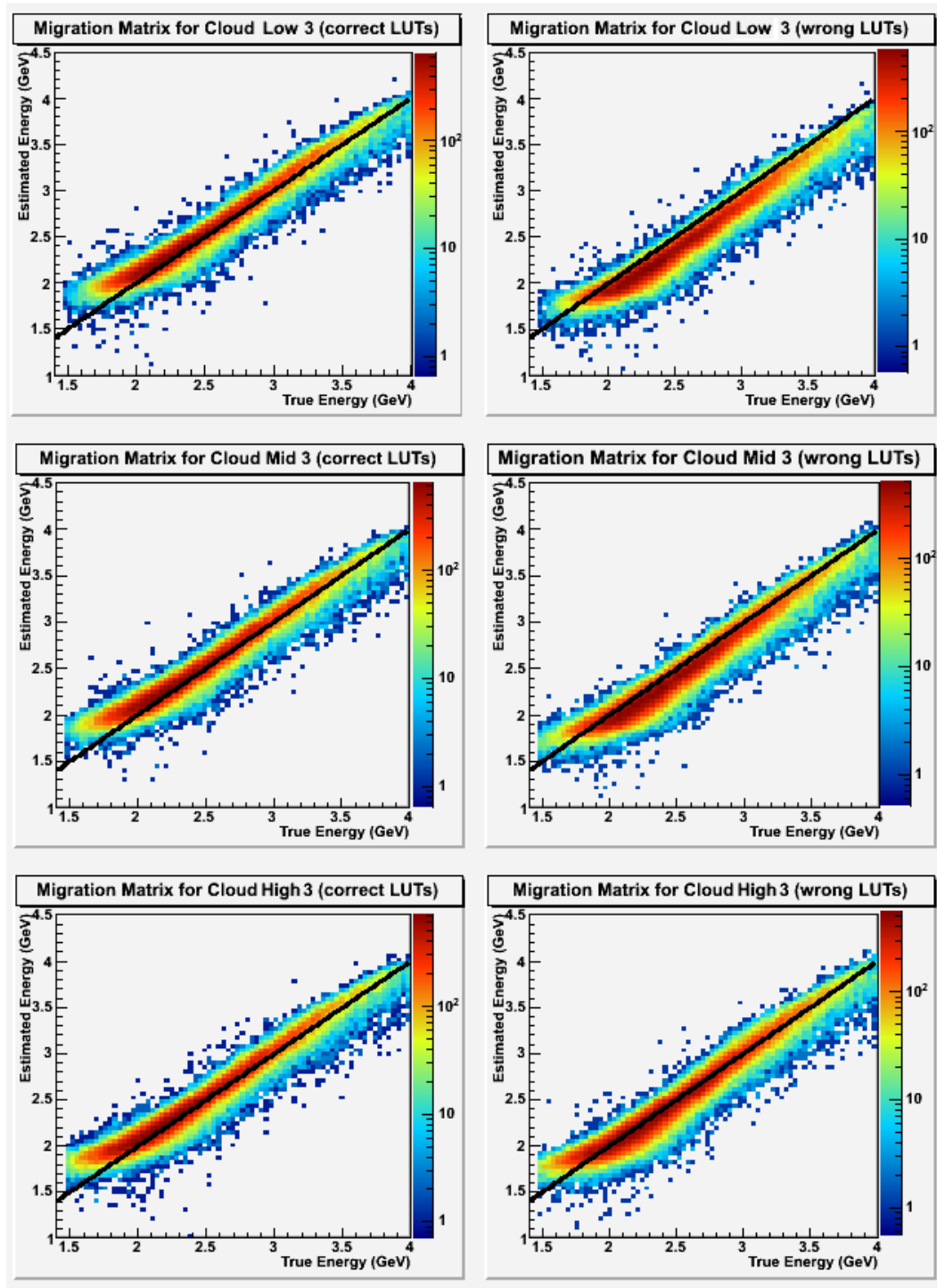


Figure 15: Estimated energy vs True energy (migration matrix) for model 4 (top), 5 (center) and 6 (down). The left column are the events analyzed with the proper MC and the column on the right are the same events but processed with standard MC (model 1). A diagonal line ( $E_{est} = E_{true}$ ) is drawn to compare with the perfect energy reconstruction case.

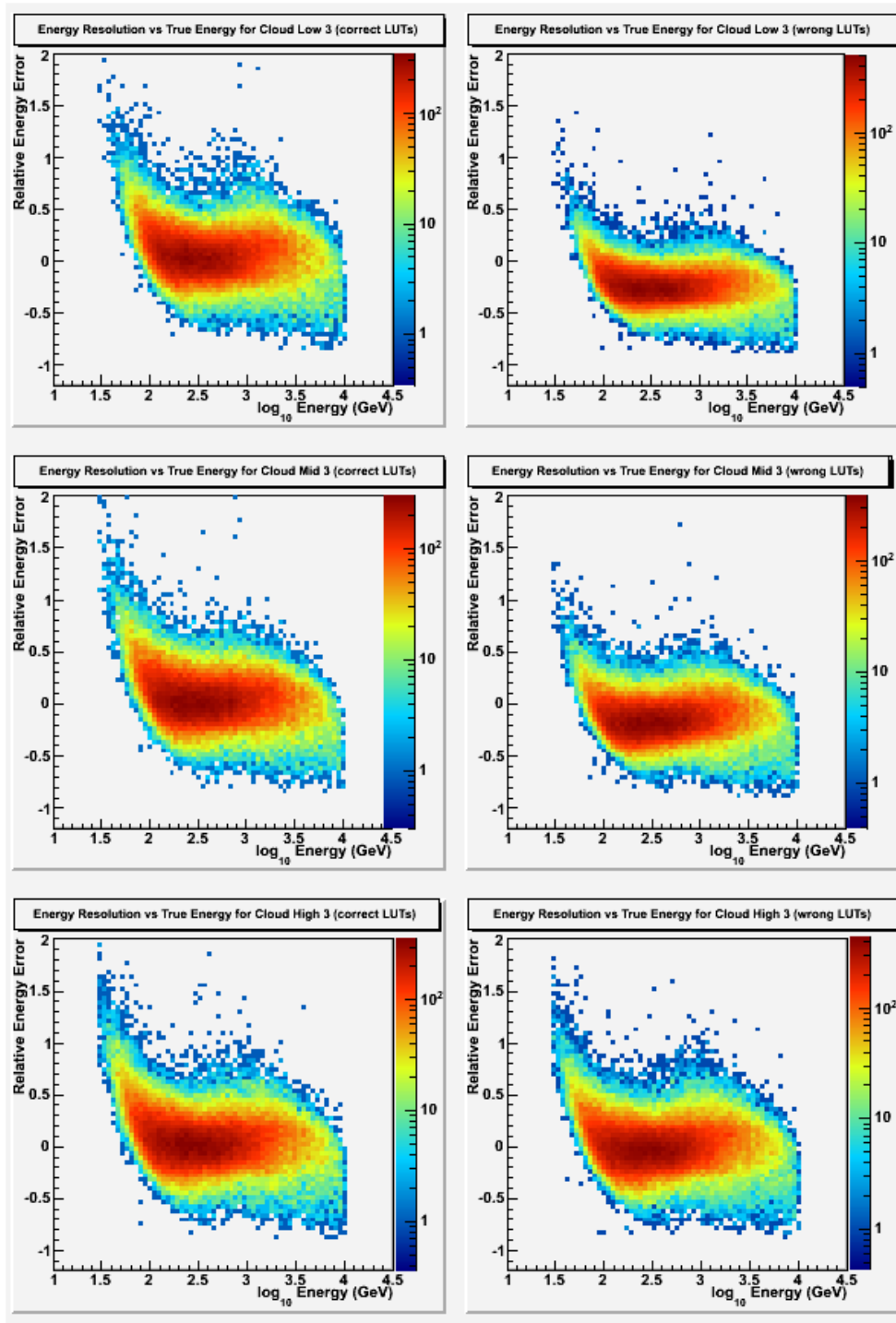
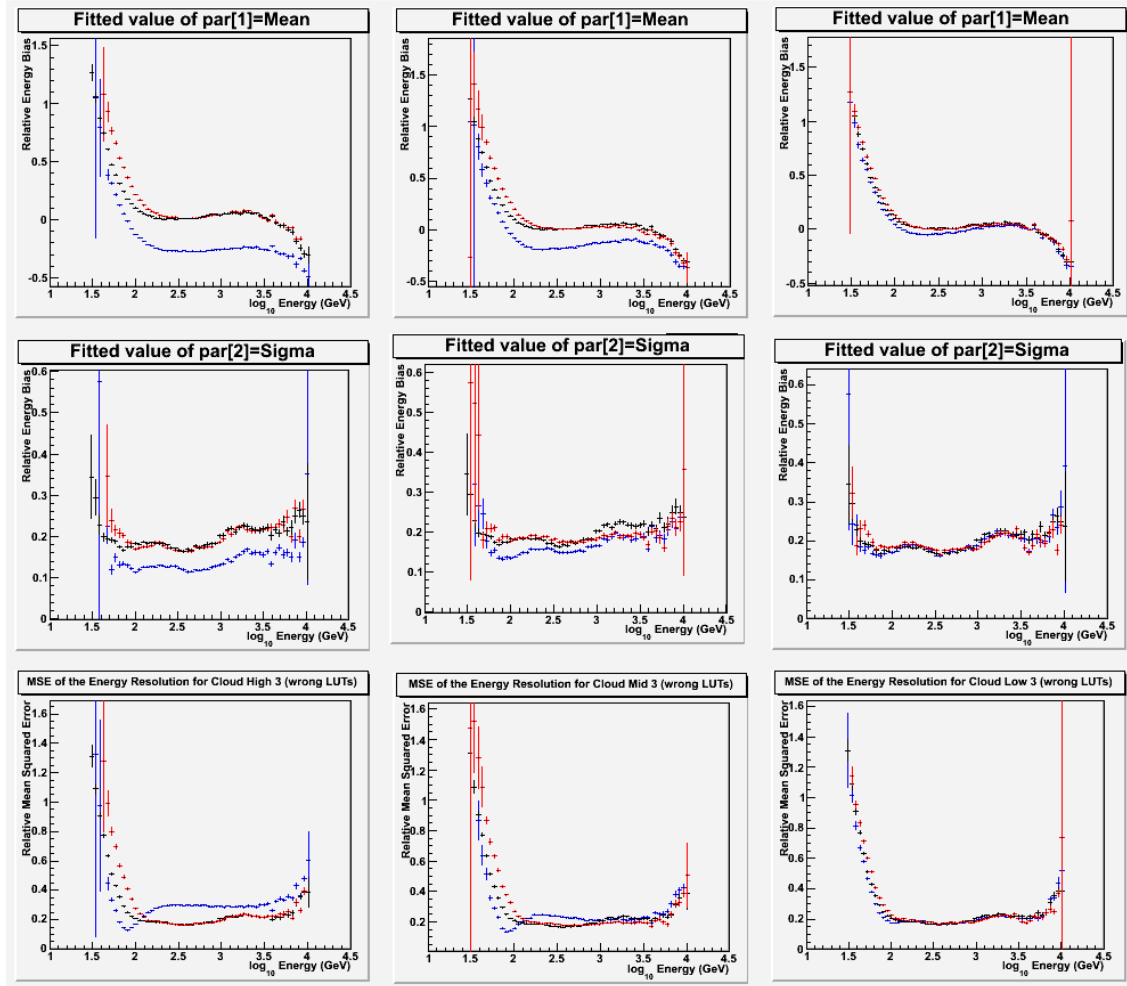


Figure 16: Relative energy error as a function of the true energy in two cases: simulated data analyzed with a properly adapted MC (*left*) and the same data analyzed with standard, model 1 MC (*right*). First row corresponds is the relative energy error for the Cloud Low 3 case (model 4), the second row is the Cloud Mid 3 case (model 5) and the third row is the Cloud High 3 case (model 6).



Model 4: Cloud Low 3

Model 5: Cloud Mid 3

Model 6: Cloud High 3

Figure 17: Relative energy bias (first row), relative energy resolution (second row) and relative mean squared error (third row). Black points represent the standard model (Elterman, model 1), red points represent models 4, 5 and 6 for each column but using adapted MC and blue points represent the same models but using standard MC (model 1) to analyze the data.

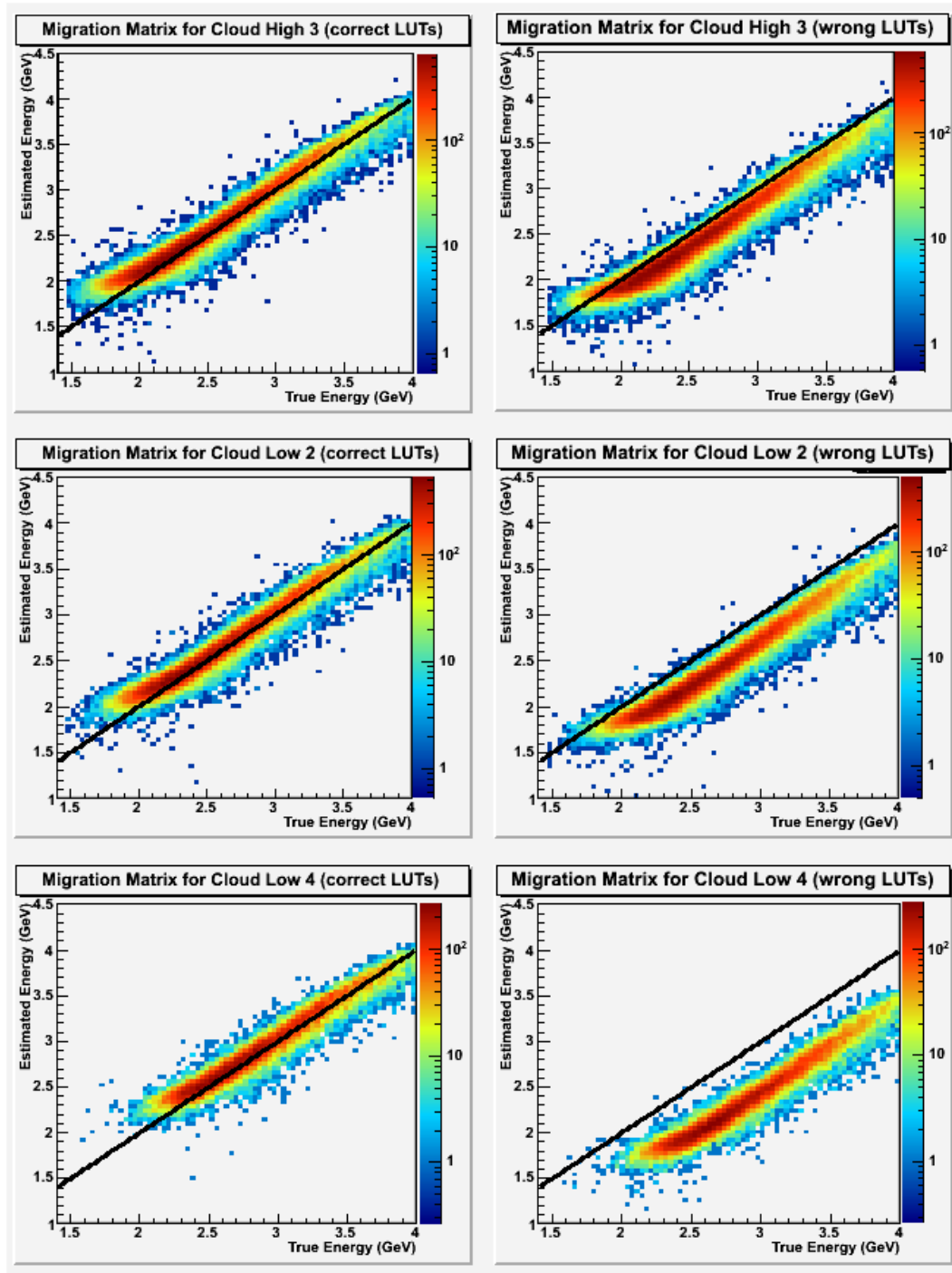


Figure 18: Estimated energy vs True energy (migration matrix) for model 4 (top), 7 (center) and 8 (down). The left column are the events analyzed with the proper MC and the column on the right are the same events but processed with standard MC (model 1). A diagonal line ( $E_{est} = E_{true}$ ) is drawn to compare with the perfect energy reconstruction case.

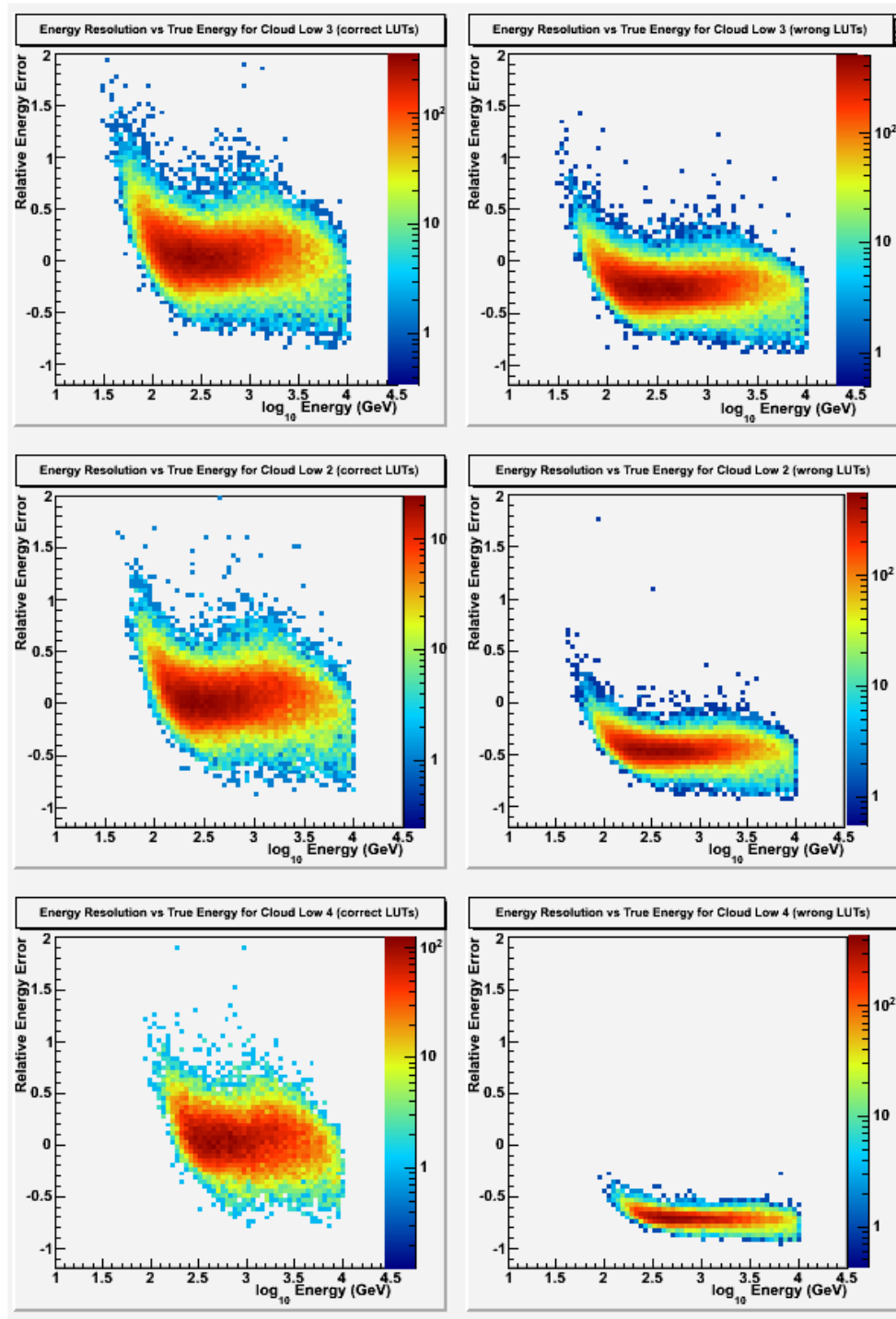
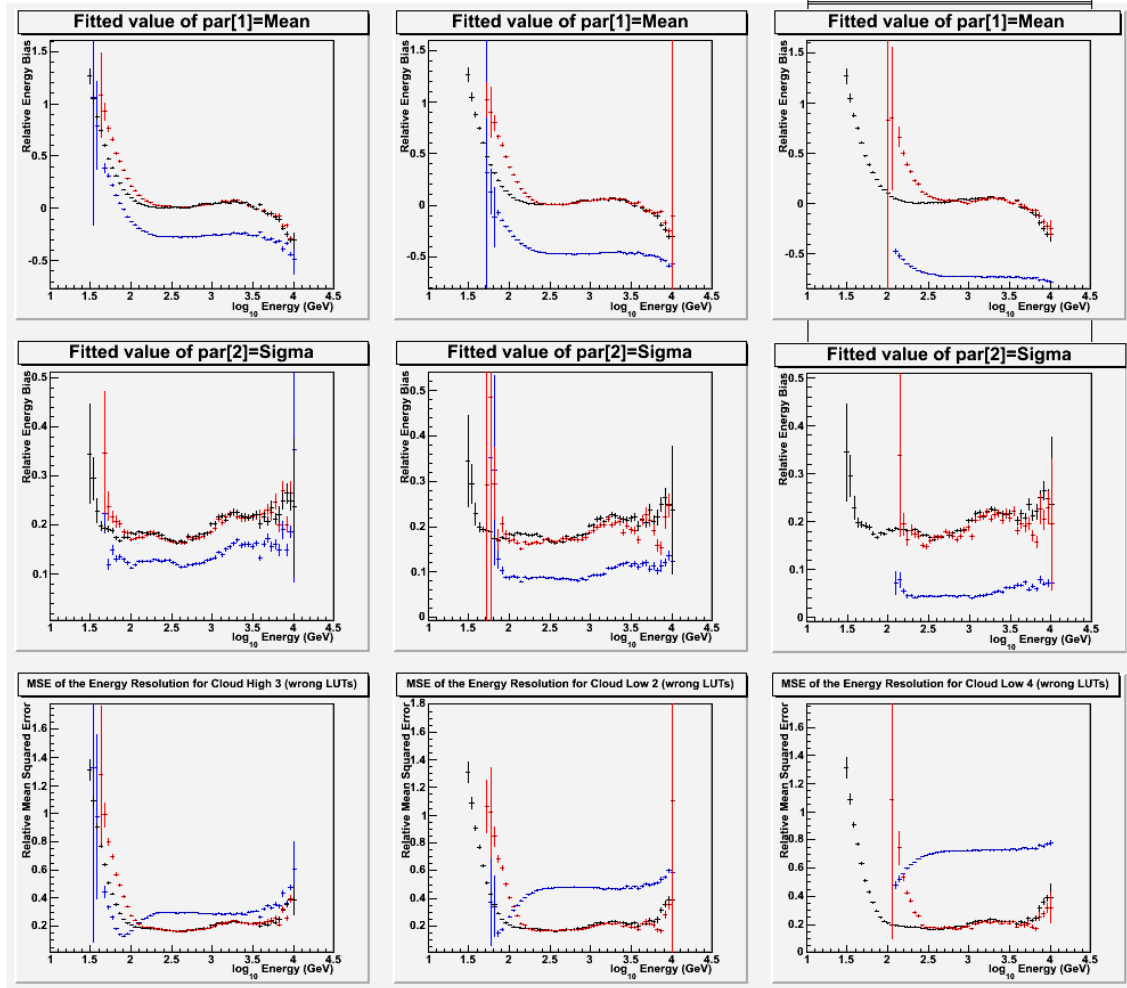


Figure 19: Relative energy error as a function of the true energy in two cases: simulated data analyzed with a properly adapted MC (*left*) and the same data analyzed with standard, model MC (*right*). First row corresponds is the relative energy error for the Cloud Low 3 (model 4), the second row is the Cloud Low 2 case (model 5) and the third row is the Cloud Low 4 case (model 6).



Model 4: Cloud Low 3

Model 7: Cloud Low 2

Model 8: Cloud Low 4

Figure 20: Relative energy bias (first row), relative energy resolution (second row) and relative mean squared error (third row). Black points represent the standard model (Elterman, model 1), red points represent models 4, 7 and 8 for each column but using adapted MC and blue points represent the same models but using standard MC (model 1) to analyze the data.

## A Figures

## B Input Cards

### B.1 Corsika Input Card

RUNNR	1	run number
PRMPAR	1	particle type
ERANGE	30. 10000.	energy range
EVTNR	1	number of first shower event
NSHOW	100	number of showers to generate
ESLOPE	-2.0	slope of primary energy spectrum
THETAP	0. 10.	range of zenith angle (degree)
PHIP	0. 0.	range of azimuth angle (degree)
DIRECT	./	data directory managed by daemon
SEED	7713279 0 0	seed values managed by daemon
SEED	3096420 0 0	seed values managed by daemon
SEED	4582915 0 0	seed values managed by daemon
OBSLEV	2200.E2	observation level (in cm)
RADNKG	200.E2	outer radius for NKG lat.dens.determ.
MAGNET	29.5 23.0	magnetic field at LaPalma
ECUTS	0.3 0.3 0.02 0.02	e.cuts: had, mu, elec y fot
MUADDI	F	additional info for muons
MUMULT	T	muon multiple scattering angle
LONGI	T 10. T F	longit.distr. & step size & fit
MAXPRT	0	max. number of printed events
ECTMAP	1.E4	cut on gamma factor for printout
STEPFC	1.0	mult. scattering step length fact.
DEBUG	F 6 F 1000000	debug flag and log.unit for out
CWAVLG	290. 900.	Cherenkov wavelength band
CSCAT	10 0. 30000.	scatter Cherenkov events
CERSIZ	1.	bunch size Cherenkov photons
CERFIL	T	Cherenkov output to extra file
DATBAS	F	write .dbase file
CERTEL	2	
	3500.0 -2400.0 0.0 0.0 0.0 2000.0 1700.0	Location and size of the CTs
	-3500.0 2400.0 0.0 0.0 0.0 2000.0 1700.0	
USER	ifae	user name
ATMOSPHERE	11 T	MAGIC Winter atmosphere with refraction
EXIT	terminates input	

### B.2 Reflector Input Card

```

reflector 0.7
#
# Sample parameters file WOBBLE+
#
verbose_level 1

```

```

#
# Seeds for random number generator:
seeds 1234566L 3141592L
#
# Define below the layout of the telescope locations as simulated in MMCS
# This command must precede the "telescope_position" commands.
# telescopes_layout Number_of_CT_systems Number_of_CTs_per_system
telescopes_layout 1 2
#
#
# Now specify the telescope locations. This must obviously be consistent with
# the locations specified in the MMCS input card, around which the C-photons
# are saved to the disk. The number of telescope_position commands must be
equal
# to the product of the two arguments of the telescopes_layout command above.
# We write first the coordinates of all the telescopes in the first system, then
# all those of the second system, and so on. The order is important! The relative
# locations of the different telescopes in each system must also be the same, for
# instance: the first telescope of each system is always the one on the SW, then
# the one in NE, or whatever. In this case it is a system of two telescopes, the
# first one is MAGIC-1, the second is the MAGIC clone, which is placed 70 m
south and
# 48 m west of the first one, that is, delta_x = -70 m, delta_y = +48 m
# telescope_position x y (in cm):
#
telescope_position 3500.0 -2400.0
telescope_position -3500.0 2400.0
#
#
# wobble_mode: possible values 0, 1, -1 (see manual). This command will be
ignored if
# the randomize_ct_orientation is also present in the input card.
#
wobble_mode 1
#
# Maximum number of events to be processed
max_events 1000000
#
# Some configuration files, and output file, for telescope 1:
#
ct_file /MagicSoft/Simulation/Detector/Data/magic.def
reflectivity_file /MagicSoft/Simulation/Detector/Data/reflectivity.dat
axisdev_file /MagicSoft/Simulation/Detector/Data/axisdev.dat
#Output1
output_file /dir/Gamma_za20to20_az00_11TCloudLow4_098_M1_w1
.rfl
# Some configuration files, and output file, for telescope 2:
#
ct_file /MagicSoft/Simulation/Detector/Data/magic2.def

```

```

reflectivity_file /MagicSoft/Simulation/Detector/Data/reflectivity.dat
axisdev_file /MagicSoft/Simulation/Detector/Data/axisdev.dat
#Output2
output_file /dir/Gamma_za20to20_az00_11TCloudLow4_098_M2_w1
.rfl
#
# ... More telescopes would follow if there are more than two telescopes per CT
system defined
# through the telescopes_layout command.
#
#
# Atmospheric model to be used in the absorption of C-photons for what regards
to Rayleigh scattering:
atm_model ATM_MagicWinter
#
# List of input file (one file per line)
# The two numbers after the filename indicate the first and the last event of
# the file to be processed. They are optional; if not set, all the events in
# each file will be processed.
#
cer_files
/dir/cer000971
/dir/cer000972
/dir/cer000973
/dir/cer000974
/dir/cer000975
/dir/cer000976
/dir/cer000977
/dir/cer000978
/dir/cer000979
/dir/cer000980
#

```

### B.3 Camera Input Card

```

camera 0.85
#-----
# Input card for Stereo simulations with different values per telescope
#-----
#
#-----
# Common values for camera simulation
#-----
#
# format version (Use 5 for Siegen FADC simulation, 9 for MUX FADCs)
# (Note: 8 was for MUX FADCs before removal of the FADC slices with switching
noise)
format_version 9
#

```

```

# Number of telescopes:
ct_num 2
#
# Telescope geometry type:
ct_geom 44
#
# Project Name: MAX 40 characters and do not put spaces, use "_" instead
project_name Gamma_MW_REFL3_za20_az0_w1
#
#observation mode: "OnOff" or "Wobble"
observation_mode Wobble
#
# Switch on NSB:
nsb_on
# nsb_off
#
# Number of photons from the diffuse NSB (nphe / ns 0.1*0.1 deg2 239 m2) and
# minimum number of phe from shower required to simulate NSB:
nsb_mean 0.20 10
#
# Seeds for random number generation:
seeds 21195 21195
#
# Write to output trigger information:
write_McTrig
#
# Write to output FADC information:
write_McFadc
#
# data_file ./Gamma_zbin0_0_7_1000to1009_w0.dat
data_file /dir/Gamma_za20to20_8_98_w1.dat
#
# Starfield (see Starfieldadder program)
#starfield_file /MagicSoft/Simulation/Detector/Starfield/starfield.rfl
#
#
#-----
# MAGIC-I simulation values. Value for each input card start always with a 0
# 0==> Means the first telescope
# Values adapted to simulate M1 telescope after the 2011 upgrade. Most of them
# copied from M2 part of this input card (Daniel Garrido, Nov 2010)
#-----
#
# Quantum efficiency file for MAGIC-1:
qe_file 0 /MagicSoft/Simulation/Detector/Data/qe-hamamatsu-MAGIC2- updated.RFL.dat
#
# Light Collection efficiency file for MAGIC-1:
lcoll_file 0 /MagicSoft/Simulation/Detector/Data/LightCollection.dat
#

```

```

# PMT time jitter (sigma of gaussian, ns) of global output pulse for MAGIC-1
pmt_jitter_ns 0 0.4
#
# additional jitter because of chessboarding (ns), half of phe will be delayed with
this value for MAGIC-1
chessboarding_jitter_ns 0 0
#
# Trigger characteristics: telescope, gate length (ns), min. overlapping time (ns),
# amplitude and FWHM of (gaussian) single phe response for trigger of MAGIC-1:
trigger_prop 0 3.0 0.25 1.0 2.0
#
# To shift the pulses in the FADC window, modify the trigger delay (ns)
trigger_delay 0 20.0
#
# Fluctuations in the gain simulation of the MAGIC-1 PMTs
#set_gain_fluct 0 -1
#
# Correction to overall light collection efficiency for MAGIC-1:
mirror_fraction 0 0.75
#
# Electronic noise in FADC (sigma in ADC counts): Telescope, Inner pixels, outer
pixels, digital noise for MAGIC-1:
fadc_noise 0 20. 20. 0.
#
# Electronic noise from a file (containing possibly elec. noise from real data) for
MAGIC-1:
# fadc_noise_from_file 0 /MagicSoft/Simulation/Detector/Data/elecnoise _20070208.root
#
# Switch off electronic noise for MAGIC-1:
# elec_noise_off 0
#
# Mean pedestal per slice (ADC counts) for MAGIC-1:
fadc_pedestal 0 10000.
#
# Additional sigma of mirror spot (cm) for MAGIC-1:
sigma_xy_cm_spot 0 0.90
#
# Directory where NSB database can be found for inner and outer pixels in MAGIC-
1:
nsb_directory 0 /MagicSoft/Simulation/Detector/StarLight/M2_DOM/inner/
nsb_dir_outer 0 /MagicSoft/Simulation/Detector/StarLight/M2_DOM/inner/
#
# FADC Type for MAGIC-1:
# 0 -> Siegen
# 2 -> MUX
fadc_type 0 2
#
# FADC properties: Telescope, shape of single phe response (1 means realistic one
for Siegen FADCs, from

```

# Pulpo setup, 0 is gaussian), integral in FADC counts for 1 phe, FWHM (ns) of the single phe pulse.

# (the 3rd argument is ignored unless gaussian shape - 1st argument=0 - was chosen) :

fadc\_prop 0 0 150. 3.5

fadc\_outer 0 0 150. 3.5

#

# Telescop, FADC sampling frequency, number of FADC slices, # of bytes per slice (1 or 2)

# and minimum step in counts (we can have 2 bytes but a 10 bit FADC, in that case the

# minimum ste would be  $2^6=64$ ):

# Last two numbers are the number of slices removed from the head and the number removed

# from the tail of the total 80 slices FADC range

fadc\_GHz 0 2. 80 2 6 0 0

#

# Saturation Method in MAGIC-2:

# 0 -> Just truncate

# 1 -> Apply MUX shaping (default)

saturation\_method 0 0

#

# Saturation Value: it can be less than  $\text{pow}(2, 8*\text{nBytes})$

# Currently the saturation value in MAGIC-1 is due to the analog electronics and is 61000

saturation\_value 0 24000

#

# L1 Trigger condition: CT number, threshold (mV), multiplicity and topology:

trigger\_single 0 4 4 2

#

# Misspointing X and Y. Typically used to generate falso wobble data from ON/OFF data

#misspoint\_deg 0 0.0 0

#

# Input file for MAGIC-1:

input\_file 0 /dir/Gamma\_za20to20\_az00\_11TCloudLow4\_098\_M1\_w1.rfl

#

# root output file name for MAGIC-1:

root\_file 0 /dir/GA\_M1\_za20to20\_8\_98\_w1.root

#

#-----

# MAGIC-II simulation values. Value for each input card start always with a 1

# 1==> Means the second telescope

#-----

#

# Quantum efficiency file for MAGIC-1:

# -The following file should be used to account for mirror reflectivity of M2 with reflector files

# generated with M1 mirror reflectivity instead of M2 one.

```

qe_file 1 /MagicSoft/Simulation/Detector/Data/qe-hamamatsu-MAGIC2-updated.RFL.dat
# -The following file should be used when reflector is run with the proper M2 mirror
reflectivity
#qe_file 1 /MagicSoft/Simulation/Detector/Data/qe-hamamatsu-MAGIC2-updated.RFL.dat
#
# Light Collection efficiency file for MAGIC-2:
lcoll_file 1 /MagicSoft/Simulation/Detector/Data/LightCollection.dat
#
# PMT time jitter (sigma of gaussian, ns) of global output pulse for MAGIC-2
pmt_jitter_ns 1 0.4
#
# additional jitter because of chessboarding (ns), half of phe will be delayed with
this value for MAGIC-2
chessboarding_jitter_ns 1 0
#
# Trigger characteristics: telescope, gate length (ns), min. overlapping time (ns),
# amplitude and FWHM of (gaussian) single phe response for trigger of MAGIC-2:
trigger_prop 1 3.0 0.25 1.0 2.0
#
# To shift the pulses in the FADC window, modify the trigger delay (ns)
trigger_delay 1 20.0
#
# Fluctuations in the gain simulation of the MAGIC-2 PMTs
#set_gain_fluct 1 -2
#
# Correction to overall light collection efficiency for MAGIC-2:
mirror_fraction 1 0.75
#
# Electronic noise in FADC (sigma in ADC counts): Telescope, Inner pixels, outer
pixels, digital noise for MAGIC-2:
fadc_noise 1 20. 20. 0
#
# Electronic noise from a file (containing possibly elec. noise from real data) for
MAGIC-2:
#fadc_noise_from_file 1 /MagicSoft/Simulation/Detector/ Data/elecnoise_20070208.root
#
# Switch off electronic noise for MAGIC-2:
# elec_noise_off 1
#
# Mean pedestal per slice (ADC counts) for MAGIC-2:
fadc_pedestal 1 10000.
#
# Additional sigma of mirror spot (cm) for MAGIC-2:
sigma_xy_cm_spot 1 1.05
#
# Directory where NSB database can be found for inner and outer pixels in MAGIC-
2:
nsb_directory 1 /MagicSoft/Simulation/Detector/StarLight/M2_DOM/inner/
nsb_dir_outer 1 /MagicSoft/Simulation/Detector/StarLight/M2_DOM/inner/

```

```

#
# FADC Type for MAGIC-2:
# 0 -> Siegen
# 2 -> MUX
# There is no Domino simulation, we use MUX also for MAGIC-2!!!
fadc_type 1 2
#
# FADC properties: Telescope, shape of single phe response (1 means realistic one
for Siegen FADCs, from
# Pulpo setup, 0 is gaussian), integral in FADC counts for 1 phe, FWHM (ns) of
the single phe pulse.
# (the 3rd argument is ignored unless gaussian shape - 1st argument=0 - was
chosen) :
fadc_prop 1 0 150 3.5
fadc_outer 1 0 150. 3.5
#
# Telescop, FADC sampling frequency, number of FADC slices, # of bytes per slice
(1 or 2)
# and minimum step in counts (we can have 2 bytes but a 10 bit FADC, in that
case the
# minimum ste would be  $2^6=64$ ):
# Last two numbers are the number of slices removed from the head and the number
removed
# from the tail of the total 80 slices FADC range
fadc_GHz 1 2. 80 2 6 0 0
#
# Saturation Method in MAGIC-2:
# 0 -> Just truncate
# 1 -> Apply MUX shaping (default)
saturation_method 1 0
#
# Saturation Value: it can be less than  $\text{pow}(2, 8*\text{nBytes})$ 
# Currently we use a guessed value for MAGIC-2
saturation_value 1 24000
#
# L1 Trigger condition: CT number, threshold (mV), multiplicity and topology:
trigger_single 1 4 4 2
#
# Misspointing X and Y. Typically used to generate falso wobble data from ON/OFF
data
#misspoint_deg 1 0.0 0
#
# Input file for MAGIC-2:
input_file 1 /dir/Gamma_za20to20_az00_11TCloudLow4_098_M2_w1.rfl
#
# root output file name for MAGIC-2:
root_file 1 /dir/GA_M2_za20to20_8_98_w1.root
#
#-----

```

```
# End of input card file  
#-----  
#  
end_file
```

## References

- [AM05] Albert Ansmann and Detlef Muller. *Lidar Range-Resolved Optical Remote Sensing of the Atmosphere*, chapter 4. Springer Series in OPTICAL SCIENCES. Springer Science+Business Media Inc., 2005.
- [Ber00] Konrad Bernlohr. Impact of atmospheric parameters on the atmospheric cherenkov technique. *Astroparticle Physics*, 12(4):255–268, 2000.
- [BHM<sup>+</sup>06] A. Biland, M. Haffke, P. Majumdar, D. Sobczynska, and V. Vitale. Monte carlo production strategy for the magic-ii two-telescope system. Technical Report 06-12, MAGIC Collaboration, 2006.
- [Elt64] Louis Elterman. Parameters for attenuation in the atmospheric windows for fifteen wavelengths. *Applied optics*, 3(6):745–750, June 1964.
- [Hru08] Dario Hrupec. *Extragalactic sources of rapidly variable high energy gamma radiation*. PhD thesis, University of Zagreb, 2008.
- [Mor03] A. Moralejo. The reflector simulation program v.0.6. Technical Report 02-11, MAGIC Collaboration, 2003.
- [Nf09] S. J. Nolan and C. B. Rulten for the CTA Consortium. Studies of lidar calibration for the next generation of imaging atmospheric cherenkov telescopes. In *31st International Cosmic Ray Conference Proceedings*, September 10 2009.
- [NPR10] S. J. Nolan, G. Puhlhofer, and C. B. Rulten. Detailed studies of astronomical calibration in imaging cherenkov astronomy. *accepted by Astroparticle Physics*, September 10 2010.
- [Ree93] W. G. Rees. *Topics in Remote Sensing I: Physical Principles of Remote Sensing*. Press Syndicate of the University of Cambridge, 1st reprint edition, 1993.
- [SNT<sup>+</sup>10] M. Sicard, M. Nadzri Md Reba, S. Tomás, A. Comerón, O. Batet, C. Muñoz-Porcar, A. Rodríguez, F. Rocadenbosch, C. Muñoz-Tuñón, and J. J. Fuensalida. Results of site testing using an aerosol, backscatter lidar at the roque de los muchachos observatory. *Monthly Notices of the Royal Astronomical Society*, 405:129–142, April 9 2010.